

Link overlap influences opinion dynamics on multiplex networks: spin model approach

Cook Hyun Kim,¹ Minjae Jo,¹ J. S. Lee,² G. Bianconi,^{3,4} and B. Kahng¹

¹*CCSS, CTP and Department of Physics and Astronomy, Seoul National University, Seoul 08826, Korea*

²*School of Physics and Quantum Universe Center, Korea Institute for Advanced Study, Seoul 02455, Korea*

³*School of Mathematical Sciences, Queen Mary University of London, E1 4GF, London, United Kingdom*

⁴*Alan Turing Institute, The British Library, NW1 2DB, London, United Kingdom*

Consider a multiplex network formed by two layers indicating social interactions: the first layer is a friendship network and the second layer is a network of business relations. In this duplex network each pair of individuals can be connected in different ways: they can be connected by a friendship but not connected by a business relation, they can be connected by a business relation without being friends, or they can be simultaneously friends and in a business relation. In the latter case we say that the links in different layers overlap. These three types of connections are called multilinks and the multidegree indicates the sum of multilinks of a given type that are incident to a given node. Previous models of opinion formation on multilayer networks have mostly neglected the effect of link overlap. Here we show that link overlap can have important effects in opinion formation. Indeed, emerging pattern of opinion formation can be significantly influenced by the statistical properties of multilinks, and in particular by the multidegree distribution. To quantitatively address this problem, we study a simple spin model, called the Ashkin-Teller model including 2-body and 4-body interactions between nodes in different layers. Here we fully investigate the rich phase diagram of this model which includes a large variety of phase transitions (PTs). Indeed the phase diagram of the model displays continuous, discontinuous, successive discontinuous, and hybrid PTs.

I. INTRODUCTION

Over the past two decades, network theory [1–5] has provided the pivotal framework for characterizing the interplay between structures and dynamics of complex systems. Recently, multilayer networks [6–10] are attracting considerable scientific interest. These network of networks are able to integrate information on various types of links characterizing complex systems where interactions have different nature and connotation. Therefore, they provide a new perspective for analyzing complex social, transportation, or biological systems [11–15] etc. Multilayer networks not only have a rich correlated structure [16–19] that encodes more information than a single layer, but also sustain dynamical processes that are strongly affected by the multiplexity of the network. These dynamical processes include percolation [17, 20–23], diffusion [24, 25], epidemic spreading [26–28], and game theory [29, 30] etc.

Multiplex networks are a special class of multilayer network consisting of a set of nodes connected by M different types of links. Each network consisting of a given type of link interaction forms one of the M layers of a multiplex network.

Most social networks are multiplex. In fact, social ties have different connotations possibly indicating friends, colleagues, acquaintances and family relations, etc. Moreover, in the modern society, online social interactions can occur between different online social networks such as Twitter, Facebook and LinkedIn etc. The vast majority of data on multiplex social networks display a significant link overlap [11, 12, 16]. This property indicates that a significant fraction of pair of nodes can be connected at the same time by more than one type of interaction. For example, it might occur that a colleague is also a friend or that a two individuals might be connected at the same time in Facebook and Twitter.

The opinion dynamics on social multiplex networks have been investigated recently using spin models such as the voter

model [31–33], election models [34], and Hamiltonian spin systems [35, 37]. The observed dynamics on social multiplex networks cannot be reduced to the dynamics on a single social aggregated network that treats all the interactions of the multiplex network on an equal footing. In adaptive voter models, an absorbing and shattered fragmentation transition [32, 33] occurs in which one layer can be fragmented into two clusters of different opinions, whereas the other layer remains connected in one cluster. In election models, the competing campaigns of two parties can give rise to election outcomes in which both parties have a large electorate [34]. Additionally, the party investing more in building a connected network of supporters is more likely to win the election [34]. In studies of the opinion dynamics on multiplex networks, where different opinions can be spread across different layers, an important question is whether each node maintains coherent behavior, that is, has a similar opinion in all the layers. A spin opinion model displaying a coherence–incoherence transition was numerically investigated recently [35]. Spins are coupled within each layer to represent the interaction between one node and its neighbors on a given topic, and also across layers to represent the tendency of each node to take a coherent opinion on all the topics.

Another spin model, which illustrates the opinion formation in social networks due to the influence of interdependence between different social communities, is the Ashkin–Teller model [36]. It was studied in scale-free network and an analytical approach revealed that a rich phase diagram including the tricritical point (TP) was obtained [37]. It was considered on a duplex network with identical topology; however, the most realistic multiplex network [7] can be the case in which the layers of the bilayer network are distinct and the amount of overlap is tunable.

Here our goal is to investigate to what extent link overlap affects opinion formation in multiplex networks and whether link overlap favors coherent opinions.

We consider a duplex network formed by two layers where a dynamics on opinion formation regarding two different subjects takes place. For example, one could consider a voting model for the city council and for the national parliament. For each vote, nodes can be influenced by a different set of nodes. In the previous example, the first layer indicates the network influencing the city council vote, the second layer indicates the network determining the national vote. The link overlap has a clear effect on this opinion dynamics by coupling the two layers. In fact if two nodes are connected in both layers it is natural to assume that the simultaneous alignment of the opinions in both layers must be favored by the dynamics. This considerations allow us to model the opinion dynamics in presence of link overlap, with a spin Hamiltonian model that is a variation of the Ashkin-Teller (AT) model that we call g -AT model. The model contains two species of Ising spins, the s -spin and σ -spin, with each species of spin located on a single layer of the duplex network. The duplex network is a maximum entropy duplex network with given multidegree distribution [16] and as such it is very suitable to modulate the role of overlapping multilinks. In particular we here assume that non-overlapping multilinks and overlapping multilinks have a scale-free multidegree distribution characterized by a different power-law exponent. Here we provide a complete analytical mean-field solution to this model and we reveal the complex phase diagram of the model. We show that favoring the simultaneous alignment of the opinions of nodes connected in both layers provides a simple mechanism to generate coherence of opinions.

This paper is organized as follows: We introduce the Hamiltonian of the g -AT model and the duplex network topology under study in Sec II. In Sec. III we derive the free energy density using the mean-field approximation, we derive self-consistency equations for the order parameters by minimizing the free energy density, and from these equations we obtain the susceptibilities. In Sec. IV, we introduce the main results of this work: the rich phase diagrams containing diverse phases and phase transition (PT) boundaries in the parameter spaces. Note that the phase diagrams are richer than those of the original AT model, because the links are classified into two types: non-overlapping and overlapping links. In Sec.V, we consider the PTs specifically in the regimes $x \ll x_M$ and $x \gg x_M$, where x_M is the characteristic ratio J_4/J_2 that separate the region into two pieces, J_2 and J_4 dominant regions. In Sec. VI, we consider PTs in the regime $x \approx x_M$. Finally, we discuss the implication of our results in Sec. VII, and summarize the results in Sec. VIII.

II. MODEL AND FORMALISM

We consider a duplex network formed by N nodes $i \in \{1, 2, \dots, N\}$. Every pair of nodes (i, j) of the duplex network can be connected in multiplex ways. In order to indicate these different type of connections we use multilinks introduced in Ref. [16]. In particular we say that a pair of nodes (i, j) is connected by a multilink $(1, 0)$ if they are only connected in layer 1, they are connected by a multilink $(0, 1)$ if they are only con-

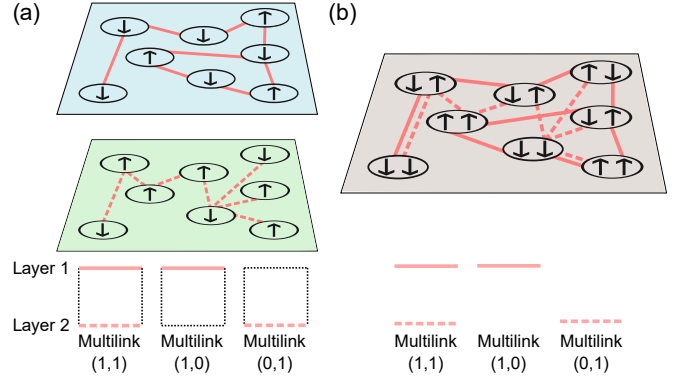


FIG. 1. (Panel (a)) The g -AT model on a duplex network: two species (s_i, σ_i) of Ising spins describe respectively the opinion in layer 1 and in layer 2. Each pair of nodes of the duplex network can be connected by a different type of multilink: multilinks $(1, 1)$ connect pair of nodes in both layer 1 and layer 2; multilinks $(1, 0)$ and $(0, 1)$ connect pair of nodes only in layer 1 and only in layer 2 respectively. Therefore multilinks $(1, 1)$ describe overlapping links while multilinks $(1, 0)$ and $(0, 1)$ describe non overlapping links. The model can be also interpreted as a model on a colored network in which nodes are associated pair of spin and the interactions between each pair of nodes can be distinguished in multilinks $(1, 1)$, $(1, 0)$ and $(0, 1)$ (panel (b)).

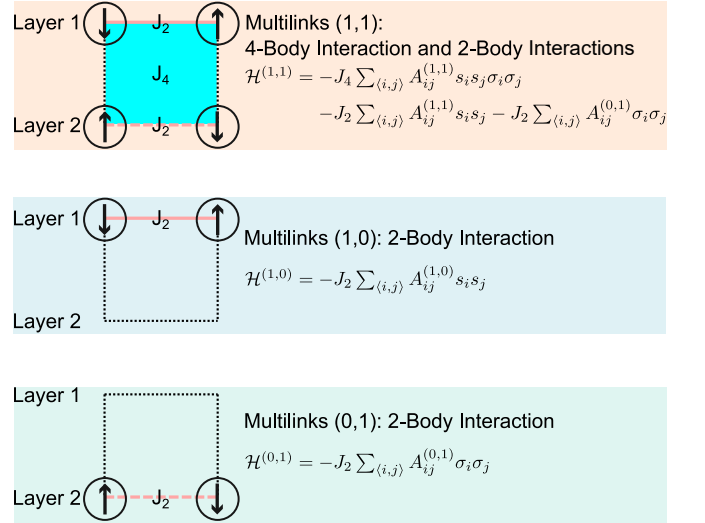


FIG. 2. The g -AT model is an Hamiltonian model combining two-body and four-body interactions. The four body interactions characterizes the interactions between the spins of species s_i , and of species σ_i connected by a multilink $(1, 1)$. The two-body interactions characterize the coupling between spins of a given species (either the spins s_i or the spins σ_i) connected by either a multilink $(1, 0)$ or a multilinks $(0, 1)$.

nected in layer 2, and they are connected by a multilink $(1, 1)$ if they are connected in both layers. Every pair of nodes can be connected only by one type of multilink, alternatively they can be unconnected in both layers (see Figure 1). We call multiadjacency matrices the matrices of elements $A_{ij}^{(1,0)}, A_{ij}^{(0,1)}, A_{ij}^{(1,1)}$ indicating whether or not the pair of nodes (i, j) is connected

by a multilink (1, 0), a multilink (0, 1) and a multilink (1, 1) respectively. This general duplex network topology includes link overlap captured by the multilinks (1, 1). The presence of such multilinks has been observed in a variety of social networks [11, 12]. Here and in the following we indicate with multidegree $k_i^{(1,0)}, k_i^{(0,1)}, k_i^{(1,1)}$ the sum of multilinks incident to the node i , i.e.

$$\begin{aligned} k_i^{(1,0)} &= \sum_{j=1}^N A_{ij}^{(1,0)}, \\ k_i^{(0,1)} &= \sum_{j=1}^N A_{ij}^{(0,1)}, \\ k_i^{(1,1)} &= \sum_{j=1}^N A_{ij}^{(1,1)}. \end{aligned} \quad (1)$$

On such a duplex network, we consider the g -AT model that describes opinion formations and takes into account the role that link overlap has on this dynamics. We consider two species of Ising spins associated to the dynamics on layer 1 and layer 2: the spin s_i are associated to the dynamics on layer 1 and take values $s_i \in \{-1, 1\}$; the spins σ_i , with $\sigma \in \{-1, 1\}$, are instead associated to the dynamics on layer 2. These spin variables are interacting via 2-body interactions and 4-body interactions (see Figure 2). In particular, for each multilink (1, 0) connecting node i to node j , we have a 2-body Ising interaction between the spins s_i and s_j with coupling constant J_2 . Similarly, for each multilink (0, 1) connecting node i to node j , we have a 2-body Ising interaction between the spins σ_i and σ_j with coupling constant J_2 . For each multilinks (1, 1) instead we consider a combination of 2-body and 4-body interactions, the 2-body interactions tend to align spins associated to the same layer with coupling constant J_2 , the 4-body interactions couples instead the four spins $s_i, s_j, \sigma_i, \sigma_j$ and is modulated by a coupling constant J_4 . In particular the Hamiltonian of the g -AT model without an external magnetic field is expressed as the sum of three terms

$$\begin{aligned} \mathcal{H}_o &= \mathcal{H}^{(1,0)} + \mathcal{H}^{(0,1)} + \mathcal{H}^{(1,1)} \\ \mathcal{H}^{(1,0)} &= -J_2 \sum_{\langle i,j \rangle} A_{ij}^{(1,0)} s_i s_j \\ \mathcal{H}^{(0,1)} &= -J_2 \sum_{\langle i,j \rangle} A_{ij}^{(0,1)} \sigma_i \sigma_j \\ \mathcal{H}^{(1,1)} &= -J_4 \sum_{\langle i,j \rangle} A_{ij}^{(1,1)} s_i s_j \sigma_i \sigma_j \\ &\quad - J_2 \sum_{\langle i,j \rangle} A_{ij}^{(1,1)} s_i s_j - J_2 \sum_{\langle i,j \rangle} A_{ij}^{(0,1)} \sigma_i \sigma_j, \end{aligned} \quad (2)$$

where $\langle i, j \rangle$ indicates the pairs of connected nodes. Alternatively the Hamiltonian \mathcal{H}_o of the g -AT model without an external magnetic field can be expressed more concisely as

$$-\beta \mathcal{H}_o = K_2 \sum_{\langle i,j \rangle} \mathbf{s}_i^T \mathbf{A}_{ij} \mathbf{s}_j, \quad (3)$$

where $\mathbf{s}_i = (s_i, \sigma_i, s_i \sigma_i)^T$, and the matrix \mathbf{A}_{ij} is given by

$$\mathbf{A}_{ij} = \begin{pmatrix} A_{ij}^{(1,0)} + A_{ij}^{(1,1)} & 0 & 0 \\ 0 & A_{ij}^{(0,1)} + A_{ij}^{(1,1)} & 0 \\ 0 & 0 & x A_{ij}^{(1,1)} \end{pmatrix}, \quad (4)$$

where $x \equiv J_4/J_2$. Moreover, $\beta = 1/k_B T$, where k_B is the Boltzmann constant, T is the temperature, $K_2 = \beta J_2$, and $K_4 = \beta J_4$ with coupling constants J_2 and J_4 .

Here, we investigate the critical properties of this model on a maximum entropy duplex network model with given multidegree distribution [16]. In order to distinguish between multilinks (1, 1) which imply link overlap and the other multilinks (1, 0) and (0, 1) which do not, we assume for simplicity that each node i of the multiplex network has the same multidegree (1, 0) and multidegree (0, 1), and we indicate the multidegree of non-overlapping multilinks and of overlapping multilinks as

$$\begin{aligned} k_i^{(1,0)} &= k_i^{(0,1)} = k_{n,i}, \\ k_i^{(1,1)} &= k_{o,i}. \end{aligned} \quad (5)$$

where the subscript n of $k_{n,i}$ indicates *non-overlap multilinks* and the subscript o of $k_{o,i}$ indicates *overlapping multilinks*. We assume that the degree distribution of each non-overlapping multilink is power-law with power-law exponent λ_n , i.e.

$$P_d(k_n) \sim (k_n)^{-\lambda_n} \quad (6)$$

The multidegree distribution of overlapping multilinks (1, 1) is also taken to be power-law but with a different exponent λ_o , i.e.

$$P_d(k_o) \sim (k_o)^{-\lambda_o}. \quad (7)$$

In the considered ensemble of duplex networks [16] a pair of nodes (i, j) is connected by (1, 0) multilinks with probability $p_{ij}^{(1,0)}$, by (0, 1) multilinks with probability $p_{ij}^{(0,1)}$ and by (1, 1) multilinks with probability $p_{ij}^{(1,1)}$ where we have

$$\begin{aligned} p_{ij}^{(1,0)} &= \frac{k_i^{(1,0)} k_j^{(1,0)}}{\langle k^{(1,0)} \rangle N}, \\ p_{ij}^{(0,1)} &= \frac{k_i^{(0,1)} k_j^{(0,1)}}{\langle k^{(0,1)} \rangle N}, \\ p_{ij}^{(1,1)} &= \frac{k_i^{(1,1)} k_j^{(1,1)}}{\langle k^{(1,1)} \rangle N}, \end{aligned} \quad (8)$$

where $\langle k^{(1,0)} \rangle$, $\langle k^{(0,1)} \rangle$ and $\langle k^{(1,1)} \rangle$ are the average multidegrees. Indeed these marginal probabilities are obtained in the maximum entropy ensemble with given multidegree distribution as long as the degree distribution display the structural cutoff. Here, we consider the thermodynamic limit ($N \rightarrow \infty$), so that the effect of structural cutoff can be ignored.

The phase diagram of this model will be affected by the topology of multiplex network and the strength of the inter-layer interaction and can be studied as a function of four parameters, λ_n , λ_o , and $x \equiv J_4/J_2$, respectively.

This g -AT model reduces to the original AT model studied in Ref. [37]. This original AT model comprises the two species of Ising spins, s_i and σ_i , locating at each site i on a monolayer network. An edge between two nodes is one type and all interactions are regarded as overlapping links (or multilinks (1, 1) from the perspective of the g -AT model. Thus, in that context a single degree exponent λ is defined.

III. MEAN-FIELD SOLUTION OF THE MODEL

To obtain the Landau free energy, we calculate the Hamiltonian in Eq. (4) by the mean-field approximation. We first take the local order parameters $\mathbf{m}_i = (m_i^s, m_i^\sigma, m_i^{s\sigma})^T$, whose components are defined as $m_i^s = \langle s_i \rangle$, $m_i^\sigma = \langle \sigma_i \rangle$, and $m_i^{s\sigma} = \langle s_i \sigma_i \rangle$. Here $\langle \dots \rangle$ is the ensemble average of a given quantity. Next, we expand each spin variable with respect to the respective local order parameter as $s_i = (m_i^s + \delta m_i^s, m_i^\sigma + \delta m_i^\sigma, m_i^{s\sigma} + \delta m_i^{s\sigma})^T$. We can neglect the higher-order terms in δm_i^s , δm_i^σ , and $\delta m_i^{s\sigma}$ because the magnitude of these terms is very small compared to that of the local order parameter. The mean-field Hamiltonian \mathcal{H}_{mf} can be written as

$$-\beta\mathcal{H}_{\text{mf}} \simeq -K_2 \sum_{i,j} \mathbf{m}_i^T \mathbf{A}_{ij} \mathbf{m}_j + K_2 \sum_{i,j} \mathbf{m}_i^T \mathbf{A}_{ij} (\mathbf{s}_j + \boldsymbol{\sigma}_j). \quad (10)$$

Then, we obtain the mean-field Landau free energy \mathcal{F} , which is given by

$$\begin{aligned} \beta\mathcal{F} &= -\ln Z \\ &= -\ln \sum_{\{s_i, \sigma_i\}} e^{-\beta\mathcal{H}_{\text{mf}}} \simeq -\sum_i \ln Z_i + K_2 \sum_{i,j} \mathbf{m}_i^T \mathbf{A}_{ij} \mathbf{m}_j \end{aligned} \quad (11)$$

where

$$Z_i = 4 [C_i(s)C_i(\sigma)C_i(s\sigma) + S_i(s)S_i(\sigma)S_i(s\sigma)], \quad (12)$$

with

$$C_i(s) \equiv \cosh \left(\sum_{j \in \text{nn}(i)} K_2 m_j^s \right), \quad S_i(s) \equiv \sinh \left(\sum_{j \in \text{nn}(i)} K_2 m_j^s \right). \quad (13)$$

Here $\sum_{j \in \text{nn}(i)}$ indicates that the summation runs over all the nearest neighbors j of node i for each of the three types of links.

Next, we use the annealed approximation to perform the summation:

$$\begin{aligned} \sum_{\langle i,j \rangle} A_{ij}^{(1,0)} \mathcal{A}_{ij} &\rightarrow \frac{1}{2} \sum_{i,j} p_{ij}^{(1,0)} \mathcal{A}_{ij}, \\ \sum_{\langle i,j \rangle} A_{ij}^{(0,1)} \mathcal{A}_{ij} &\rightarrow \frac{1}{2} \sum_{i,j} p_{ij}^{(0,1)} \mathcal{A}_{ij} \quad \text{and} \\ \sum_{\langle i,j \rangle} A_{ij}^{(1,1)} \mathcal{A}_{ij} &\rightarrow \frac{1}{2} \sum_{i,j} p_{ij}^{(1,1)} \mathcal{A}_{ij}, \end{aligned} \quad (14)$$

where \mathcal{A}_{ij} is a given function of i and j and $p_{ij}^{(1,0)}$, $p_{ij}^{(0,1)}$ and $p_{ij}^{(1,1)}$ are defined in Eq. (9).

We define a global order magnetization for s spin :

$$m_s^{(1,0)} = \frac{\sum_i k_i^{(1,0)} m_i^s}{N \langle k^{(1,0)} \rangle} \quad \text{and} \quad m_s^{(1,1)} = \frac{\sum_i k_i^{(1,1)} m_i^s}{N \langle k^{(1,1)} \rangle}, \quad (15)$$

where m_i^s is the local order parameter for s spin. We introduce global order parameters for σ and $s\sigma$ spins similarly. Then, we set that $M \equiv m_{s\sigma}^{(1,1)}$.

Since the considered duplex network ensemble has the same multidegree distribution of the non-overlapping multilinks we can set

$$m_s^{(1,0)} = m_\sigma^{(0,1)} \equiv m_n, \quad m_s^{(1,1)} = m_\sigma^{(1,1)} \equiv m_o. \quad (16)$$

The three order parameters are now denoted as m_o , m_n , and M -magnetization, respectively. Applying the annealed approximation, we rewrite the free energy density ($f \equiv \beta\mathcal{F}/N$) in terms of the order parameters m_n , m_o , and M . The free energy density f is given by

$$\begin{aligned} f &\simeq K_2 m_n^2 \langle k_n \rangle + K_2 m_o^2 \langle k_o \rangle + \frac{1}{2} K_4 M^2 \langle k_o \rangle \\ &- 2 \int_{k_{\min}^n}^{\infty} \int_{k_{\min}^o}^{\infty} dk_n dk_o P_d(k_n) P_d(k_o) \ln [\cosh (K_2 (m_n k_n + m_o k_o))] \\ &- \int_{k_{\min}^o}^{\infty} dk_o P_d(k_o) \ln [\cosh (K_4 M k_o)] - \mathcal{B}_1, \end{aligned} \quad (17)$$

where

$$\mathcal{B}_1 = \int_{k_{\min}^n}^{\infty} \int_{k_{\min}^o}^{\infty} dk_n dk_o P_d(k_n) P_d(k_o) \ln (1 + \mathcal{T}_2^2 \mathcal{T}_4), \quad (18)$$

with

$$\mathcal{T}_2 \equiv \tanh (K_2 (m_n k_n + m_o k_o)), \quad \mathcal{T}_4 \equiv \tanh (K_4 M k_o). \quad (19)$$

Minimizing the free energy, $\partial f / \partial m_a = 0$ and $\partial f / \partial M = 0$, we obtain the following self-consistency relations:

$$m_a \langle k_a \rangle = \int_{k_{\min}^n}^{\infty} \int_{k_{\min}^o}^{\infty} dk_n dk_o P_d(k_n) P_d(k_o) \frac{\mathcal{T}_2 (1 + \mathcal{T}_4)}{1 + \mathcal{T}_2^2 \mathcal{T}_4} k_a \quad (20)$$

where a represents o or n index, and

$$M \langle k_o \rangle = \int_{k_{\min}^n}^{\infty} \int_{k_{\min}^o}^{\infty} dk_n dk_o P_d(k_n) P_d(k_o) \frac{\mathcal{T}_4 + \mathcal{T}_2^2}{1 + \mathcal{T}_2^2 \mathcal{T}_4} k_o. \quad (21)$$

The self-consistency equations Eqs. (20) and (21) admit three solutions, corresponding to the paramagnetic phase ($m_a = 0, M = 0$), the Baxter phase ($m_a > 0, M > 0$), and the $\langle \sigma s \rangle$ phase ($m_a = 0, M > 0$).

To obtain the susceptibility, we also consider a Hamiltonian including an external magnetic field, given by

$$-\beta\mathcal{H} = -\beta\mathcal{H}_o + \sum_i \mathbf{H}_i^T \mathbf{s}_i, \quad (22)$$

where $\mathbf{H}_i = (k_{o,i} H_o + k_{n,i} H_n, k_{o,i} H_o + k_{n,i} H_n, k_{o,i} H_4)^T$; and H_a is external magnetic field applied to s and σ spins in proportion to the multidegree k_a ; and H_4 is another external magnetic

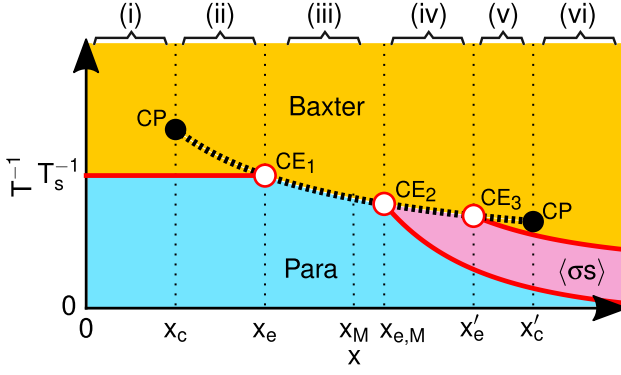


FIG. 3. Schematic phase diagram of the g -AT model for a given set of $\lambda_n = 3.53$ and $\lambda_o = 3.90$. Solid and dotted curves represent continuous and discontinuous PTs, respectively. This phase diagram is mostly similar to the one of the original AT model [37].

field applied to $s\sigma$ spins in proportion to degree k_o . Minimizing the free energy, we obtain the self-consistency equations for magnetizations with respect to external magnetic fields:

$$-\frac{\partial f}{\partial H_a} = m_a \langle k_a \rangle, \quad -\frac{\partial f}{\partial H_4} = M \langle k_o \rangle. \quad (23)$$

These self-consistency equations can be obtained by substituting $K_2 m_a k_a$ and $K_4 M k_o$ with $(K_2 m_a + H_a) k_a$ and $(K_4 M + H_4) k_o$, respectively, in Eqs. (17), (18), (20), and (21) (see Appendix A). The susceptibilities are calculated using the following relations:

$$\chi_a \equiv \left. \frac{\partial m_a}{\partial H_a} \right|_{H_a, H_4 \rightarrow 0}, \quad \chi_M \equiv \left. \frac{\partial M}{\partial H_4} \right|_{H_a, H_4 \rightarrow 0}. \quad (24)$$

Using the above relation, the susceptibilities χ can be obtained as follows:

$$\chi_a = \frac{\mathcal{A}_{aa} + \mathcal{A}_{a\bar{a}} K_2 \partial m_{\bar{a}} / \partial H_a + \mathcal{A}_{aM} K_4 \partial M / \partial H_a}{\langle k_a \rangle - K_2 \mathcal{A}_{aa}}, \quad (25)$$

$$\chi_M = \frac{\mathcal{A}_{MM} + \mathcal{A}_{M\bar{o}} K_2 \partial m_{\bar{o}} / \partial H_4 + \mathcal{A}_{Mn} K_2 \partial m_n / \partial H_4}{\langle k_o \rangle - K_4 \mathcal{A}_{MM}}, \quad (26)$$

where $a \in \{n, o\}$ and $\bar{a} \in \{n, o\}$ with a different from \bar{a} . Here the \mathcal{A} terms are obtained as follows

$$\mathcal{A}_{aa} = \frac{\partial m_{a1}}{\partial H_a}, \quad \mathcal{A}_{a\bar{a}} = \frac{\partial m_{a1}}{\partial H_{\bar{a}}}, \quad \mathcal{A}_{aM} = \frac{\partial m_{a1}}{\partial H_4},$$

$$\mathcal{A}_{Ma} = \frac{\partial M_1}{\partial H_a} \text{ and } \mathcal{A}_{MM} = \frac{\partial M_1}{\partial H_4}. \quad (27)$$

In Appendix B we provide the extensive formulas for \mathcal{A} s in the limit in which $H_a \rightarrow 0$ and $H_4 \rightarrow 0$, when m_{a1} and M_1 represent integral terms in Eqs. (A2) and Eqs. (A3).

IV. MAIN RESULTS

In order to characterize properties of the g -AT model here we discuss the phase diagram in the parameter space $[x, T^{-1}]$ for a given value of the power-law exponents $\lambda_n = 3.53$ and

$\lambda_o = 3.90$ (see Fig. 3). This choice of parameters yields a phase diagram similar to the phase diagram of the original AT model [37] in the range $\lambda_c < \lambda < 4$, where λ is the degree exponent of the scale free (SF) network on which the two species of spins lie. The SF network of the original AT model is composed of only overlapping links. $\lambda_c \approx 3.503$ is a TP of the original AT model [37], above which a discontinuous PT occurs when the ratio between J_2 and J_4 interactions strength is unity ($x = 1$). Note that when $x = 1$, i.e., $J_2 = J_4$, the Hamiltonian for the original AT model,

$$\mathcal{H} = -J_2 \sum_{\langle ij \rangle} (s_i s_j + \sigma_i \sigma_j) - J_4 \sum_{\langle ij \rangle} s_i s_j \sigma_i \sigma_j, \quad (28)$$

can be rewritten in the form of the 4-state Potts model as

$$\mathcal{H} = -4J_2 \sum_{\langle ij \rangle} (\delta(q_i, q_j) - 1/4), \quad (29)$$

where q_i is a Potts spin with 0, 1, 2 or 3 at site i and $\delta(q_i, q_j) = 1$ for $q_i = q_j$, and zero otherwise [38].

This phase diagram contains a paramagnetic phase ($m_a = 0, M = 0$) (denoted as “Para”) in high temperature region, a Baxter phase ($m_a > 0, M > 0$), and a $\langle \sigma s \rangle$ phase ($m_a = 0, M > 0$). Dotted and solid phase boundary curves represent discontinuous and continuous PTs, respectively. T_s is a critical temperature, across which a second-order PT occurs from the Para phase to the Baxter phase. T_s is independent of the ratio between J_2 and J_4 interaction strengths x for $x < x_e$.

The phase diagram has distinct critical points: two CPs and three CEs. CP represents a critical point, at which the first-order transition curve (denoted by dotted curve) terminates. CE displays a critical endpoint, indicating the end of a line of continuous PTs which is located in the middle of a line indicating first-order transitions. We will show that a mixed-order (or hybrid) transition occurs at this point. There exist two CPs and three CEs in Fig. 3. Their x positions are asymmetric. Actually, the phase diagram can be divided into two parts with respect to x_M . Here x_M indicates a characteristic ratio between J_2 and J_4 . For $x < x_M$, the J_2 interactions are dominant, $O(m_a) \gg O(M)$ near transition temperature. On the other hand, for $x > x_M$, J_4 interactions (interlayer interaction) become dominant and $O(m_a) \ll O(M)$ near transition temperature. Thus, $\langle \sigma s \rangle$ phase emerges. For the original AT model, $x_M = 1$; however, for the g -AT model, x_M depends on λ_n and λ_o . x_M locates between x_e and $x_{e,M}$ in Fig. 3. Explicitly formula to derive x_M will be presented in Eq. (34).

The phase diagram is divided into six regions based on the ratio x :

- (i) In the region (i), a continuous PT occurs at T_s for m_a and M , ((i)-type PT).
- (ii) in the region (ii), a continuous PT occurs at T_s for m_a and M . As T is decreased further, a discontinuous PT occurs subsequently at T_f , ((ii)-type PT).
- (iii) in the region (iii), a discontinuous PT occurs at T_f for m_a and M , ((iii)-type PT).

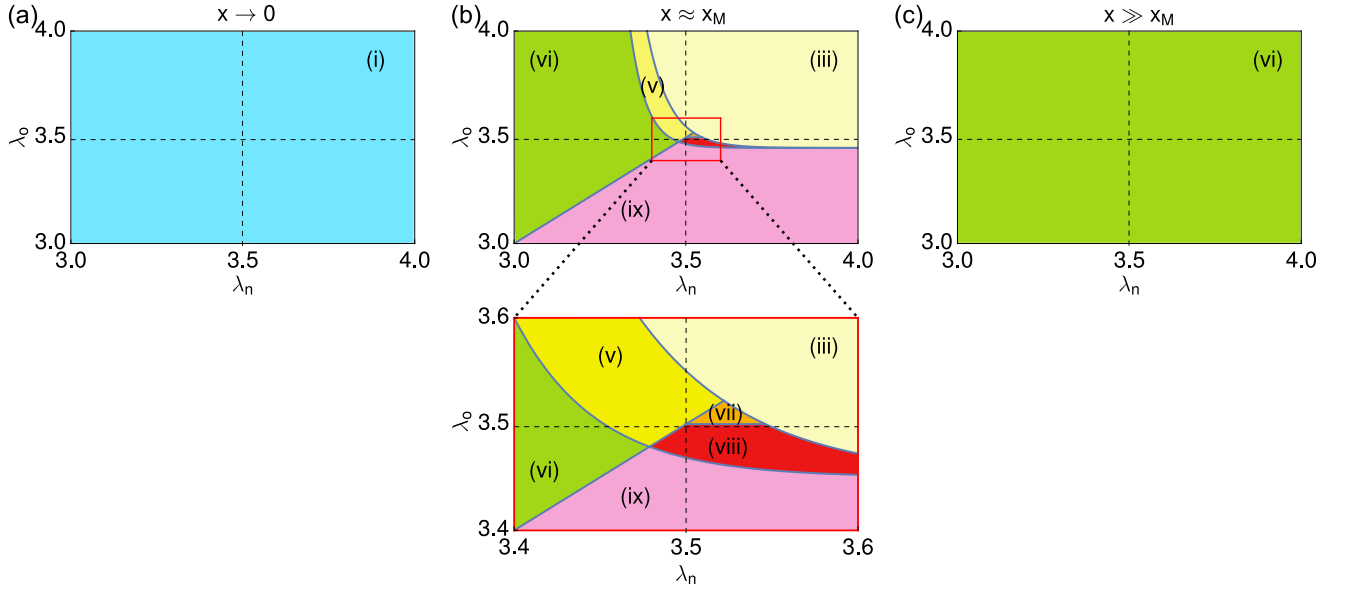


FIG. 4. Schematic phase diagrams of the g -AT model in the parameter space $[\lambda_n, \lambda_o]$ for (a) $x \approx 0$, (b) $x = x_M$, and (c) $x \gg x_M$. The notations of the phases (i)–(vii) are the same as the ones presented in Figs. 3 and 5.

- (iv) in the region (iv), a continuous PT occurs for M at $T_{s,M}$. As T is decreased further, a discontinuous PT occurs at T_f for m_a and M , ((iv)-type PT).
- (v) in the region (v), two continuous PTs occur successively at $T_{s,M}$ for M and T'_s for m_a , respectively. Then a discontinuous PT occurs at T_f for m_a and M as T is decreased further, ((v)-type PT).
- (vi) in the region (vi), two continuous PTs occur at $T_{s,M}$ for M and at T'_s for m_a , respectively, ((vi)-type PT).

The phase diagram also depends on the degree exponent λ_n and λ_o , denoted as (λ_n, λ_o) hereafter. For all (λ_n, λ_o) , a PT of (i)-type occurs in the region $x \rightarrow 0$ [Fig. 4(a)] and a PT of (vi)-type occurs in the region $x \gg x_M$ [Fig. 4(c)]. Around $x = x_M$, a rich phase diagram is created in the space (λ_n, λ_o) [Fig. 4(b)], depending on the relative magnitudes among λ_n , λ_o , and $\lambda_c \approx 3.503$. For a fixed $\lambda_n > \lambda_c$, say $\lambda_n = 3.6$, as λ_o is decreased, the type of PT changes from a first-order to the type of region (ix) through the type of region (viii) (Fig. 4(b)). (ix)- and (viii)-type of PTs are the same as (i)- and (ii)-type of PTs defined in Fig. 3, respectively, except the critical exponents for M . Detailed discussion is presented in Sec. IV. Particularly, when λ_n is slightly larger than λ_c , the PT type changes from a first-order to a second-order through two regions (vii) and (viii). In the region (vii), two discontinuous PTs occur successively as T is decreased, which is depicted in Fig. 5(f). On the other hand, when λ_o is fixed in the region larger than λ_c , as λ_n is decreased, the PT type changes from a first-order to (v), and then (vi), successively.

In order to explore the dependence of this rich phase diagram on the exponents λ_n and λ_o around $x = x_M$, we plot the phase diagram in the space $[x, T^{-1}]$ for various values of the degree pairs (λ_n, λ_o) (see Fig. 5). We find that if a first-order PT occurs at $x = x_M$, overall phase diagram would be close

to Fig. 5(c). Meanwhile, if (ii)- and (v)-types of PTs occur at $x = x_M$, then the phase diagram is similar to Fig. 5(b) and/or (e), respectively. When $\lambda_n < \lambda_o \approx 3.90$, as λ_n is decreased, the discontinuous transition curve shrinks and moves left upward as shown in Figs. 5(a)-(c). Moreover, when λ_n is slightly larger than $\lambda_o \approx \lambda_c^+$, double discontinuous transition curves appear in the phase diagram as shown in Fig. 5(f), where two discontinuous PTs occur successively as T is decreased.

In the following section, we will investigate the nature of each PT as it is revealed by investigating the corresponding Landau free energy. In this way we will uncover the underlying mechanism for these rich phase diagrams.

V. DIVERSE TYPES OF PHASE TRANSITIONS FOR $x < x_M$ AND $x > x_M$

To investigate the critical behavior near the critical temperature, we expand the free energy density as a function of the order parameters m_a and then analyze the leading terms when m_a and M converge to 0. To proceed, it is necessary to derive the relation between m_a and M , which turns out to depend on the ratio x . For x values smaller and bigger than the characteristic ratio x_M , we observe different phenomenology. Here we discuss in the details the case $0 < x < x_M$ and the case $x > x_M$ while the case $x = x_M$ is considered more in detail in Sec. V.

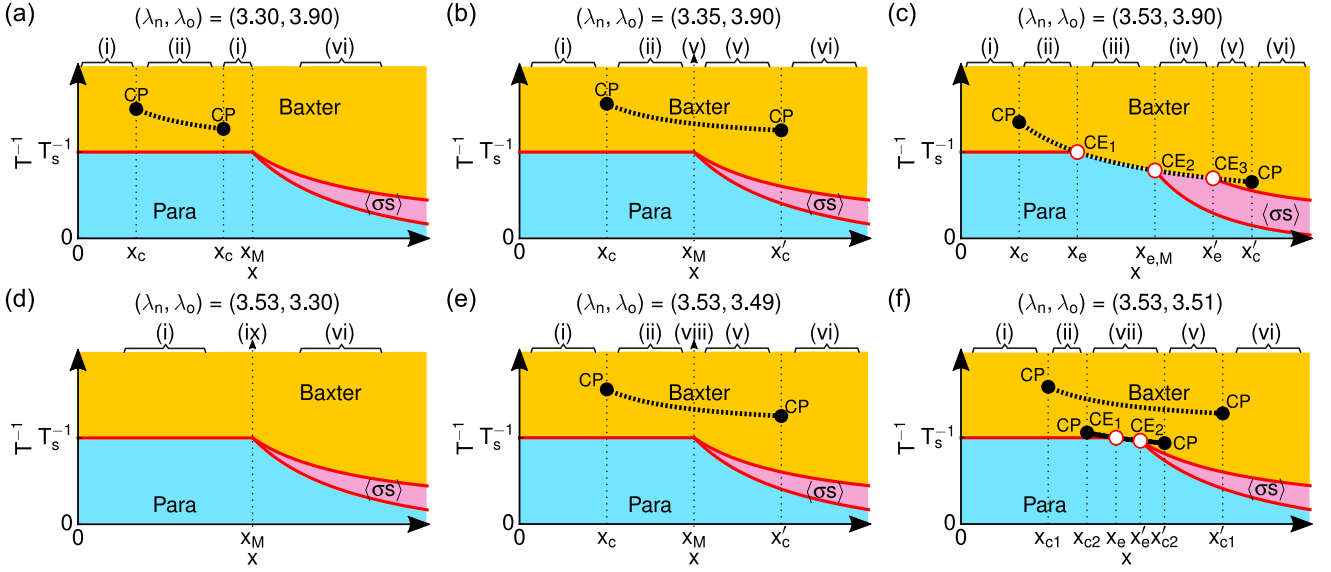


FIG. 5. Schematic phase diagrams of the g -AT model in the parameter space $[x, T_s^{-1}]$ for various values λ_n and λ_o . $(\lambda_n, \lambda_o) =$ (a) (3.30, 3.90), (b) (3.35, 3.90), (c) (3.53, 3.90), (d) (3.53, 3.30), (e) (3.53, 3.49), and (f) (3.53, 3.51).

A. When $0 < x < x_M$

For $x \in (0, x_M)$ we can expand Eqs. (20) and (21) in terms of m_a and M within the lowest order terms as follows:

$$m_n \langle k_n \rangle \left(1 - K_2 \frac{\langle k_n^2 \rangle}{\langle k_n \rangle} \right) \simeq K_2 m_o \langle k_n \rangle \langle k_o \rangle - (\lambda_n - 1) C_n(\lambda_n) (K_2 m_n)^{\lambda_n - 2} + \text{h.o.}, \quad (30)$$

$$m_o \langle k_o \rangle \left(1 - K_2 \frac{\langle k_o^2 \rangle}{\langle k_o \rangle} \right) \simeq K_2 m_n \langle k_n \rangle \langle k_o \rangle - (\lambda_o - 1) C_o(\lambda_o) (K_2 m_o)^{\lambda_o - 2} + (\lambda_o - 2) D_m(\lambda_o) (K_4 M) (K_2 m_o)^{\lambda_o - 3} + \text{h.o.}, \quad (31)$$

$$M \langle k_o \rangle \left(1 - x K_2 \frac{\langle k_o^2 \rangle}{\langle k_o \rangle} \right) \simeq D_m(\lambda_o) (K_2 m_o)^{\lambda_o - 2} - (\lambda_o - 1) C_M(\lambda_o) (K_4 M)^{\lambda_o - 2} + \text{h.o.}, \quad (32)$$

where the coefficients of the entropy terms $C_a(\lambda_a)$ and $C_M(\lambda_o)$ are derived in Appendix C. The coefficient of the interlayer interaction term $D_m(\lambda_o)$ of the r.h.s. of Eq. 31 is also derived in Appendix C. This term needs to be considered, because it is negative and contributes to the first-order transition.

To obtain T_s , we first consider the lowest-order terms of Eqs. (30) and (31) and obtain the following:

$$\left(1 - \frac{\langle k_o^2 \rangle}{\langle k_o \rangle} \frac{1}{T} \right) \left(1 - \frac{\langle k_n^2 \rangle}{\langle k_n \rangle} \frac{1}{T} \right) - \frac{1}{T^2} \langle k_n \rangle \langle k_o \rangle = 0. \quad (33)$$

This equation has two solutions of T , denoted as T_ℓ and T_h .

It is guaranteed that the l.h.s of Eq. (32) is positive as $T \rightarrow T_h^-$ as long as $x < x_M$ with

$$x_M \equiv T_h \langle k_o \rangle / \langle k_o^2 \rangle. \quad (34)$$

Then M is written within a leading order as

$$M \simeq \frac{D_m(\lambda_o)}{\langle k_o \rangle [1 - x T_h / (x_M T)]} (K_2 m_o)^{\lambda_o - 2} + \text{h.o.} \quad (35)$$

This implies that $O(M) \ll O(m_a)$ near T_h^- for $\lambda_o > 3$. Using this relation (35), we obtain the self-consistency relations for m_a with leading terms as follows:

$$m_a \langle k_n \rangle \langle k_o \rangle \left(1 - \frac{T_\ell}{T}\right) \left(1 - \frac{T_h}{T}\right) \simeq -(\lambda_a - 1)E_{\bar{a}}C_a(\lambda_a)(K_2m_a)^{\lambda_a-2} - (\lambda_{\bar{a}} - 1)F_{\bar{a}\bar{a}}C_{\bar{a}}(\lambda_{\bar{a}})(K_2m_{\bar{a}})^{\lambda_{\bar{a}}-2}, \quad (36)$$

where $E_{\bar{a}} = \langle k_{\bar{a}} \rangle \left(1 - \frac{\langle k_{\bar{a}}^2 \rangle / \langle k_{\bar{a}} \rangle}{T}\right)$ and $F_{\bar{a}\bar{a}} = \frac{1}{T} \langle k_n \rangle \langle k_o \rangle$.

As $T \rightarrow T_h^-$, $m_a \rightarrow 0$ and thus $M \rightarrow 0$ in Eq. (35). This implies that the PT from Baxter to Para phase is continuous.

(i) For $\lambda_n > \lambda_o$,

$$f(m_o) \simeq A_o K_2 m_o^2 \left(1 - \frac{T_s}{T}\right) + C_o(\lambda_o)(K_2 m_o)^{\lambda_o-1} + C_n(\lambda_n)(B_o m_o)^{\lambda_n-1} - \frac{1}{2} \frac{K_4 [D_m(\lambda_o)]^2}{\langle k_o \rangle [1 - x T_s / (x_M T)]} (K_2 m_o)^{2(\lambda_o-2)} + \text{h.o.}, \quad (37)$$

where A_o and B_o are functions of λ_a and K_2 , of which explicit formula is presented in Appendix D.

(ii) For $\lambda_n < \lambda_o$,

$$f(m_n) \simeq A_n K_2 m_n^2 \left(1 - \frac{T_s}{T}\right) + C_n(\lambda_n)(K_2 m_n)^{\lambda_n-1} + C_o(\lambda_o)(B_n m_n)^{\lambda_o-1} - \frac{1}{2} \frac{K_4 [D_m(\lambda_o)]^2}{\langle k_o \rangle [1 - x T_s / (x_M T)]} (B_n m_n)^{2(\lambda_o-2)} + \text{h.o.}, \quad (38)$$

where A_n and B_n are functions of λ_a and K_2 , of which explicit formula is presented in Appendix D. Note that $C_a(\lambda_a)$ and $D_m(\lambda_o)$ are always positive.

The phase diagram in the space of $[x, T^{-1}]$ depends on λ_n and λ_o as shown in Fig. 5. These phase diagrams reveal the nature of the observed PTs and can be obtained by examining the profiles of the Landau free energy for different x and T values for given λ_n and λ_o . To be concrete, here we consider the case of $\lambda_n = 3.53$ and $\lambda_o = 3.90$, for which we obtain the phase diagram similar to that of the original AT model with the degree exponent $\lambda > \lambda_c$.

First we observe that as $x \rightarrow 0$, a continuous PT occurs when both λ_n and λ_o are in $[3, 4]$. Both m_a and M increase continuously as T is decreased further from T_s . In this case the higher order terms of $f(m_a)$ including D_m are negligible compared to the leading terms of $f(m_a)$.

Using Eqs. (37) and (38), it is obtained that the magnetizations behave as

$$m_a \sim (T_s - T)^{\beta_m} \quad \text{with} \quad \beta_m = \frac{1}{\lambda_{\min} - 3}, \quad (39)$$

$$M \sim (T_s - T)^{\beta_M} \quad \text{with} \quad \beta_M = \frac{\lambda_o - 2}{\lambda_{\min} - 3}, \quad (40)$$

where $\lambda_{\min} = \min(\lambda_o, \lambda_n)$. The specific heat behaves as

$$C \sim (T_s - T)^{-\alpha} \quad \text{with} \quad \alpha = \frac{\lambda_{\min} - 5}{\lambda_{\min} - 3}. \quad (41)$$

The susceptibility behaves as

$$\chi_a \sim \begin{cases} (T_s - T)^{-\gamma^-} & \text{with } \gamma^- = 1 \text{ for } T < T_s, \\ (T - T_s)^{-\gamma^+} & \text{with } \gamma^+ = 1 \text{ for } T > T_s. \end{cases} \quad (42)$$

We confirm that a second-order transition occurs at T_h . This temperature is denoted as a critical temperature $T_s \equiv T_h$.

Using Eq. (35), we expand the free energy density of Eq. (17) with respect to m_a up to the three lowest order terms:

The derivation of χ_a is presented in Appendix E.

Secondly we observe that, as x is increased but still remains less than x_M , the absolute magnitude of the 4th term, called the D_m term, increases and becomes comparable to the magnitude of the C_a term. Then a first-order transition occurs in the region (ii) $x_c < x < x_e$ in Fig. 3. As temperature is lowered than T_s , the absolute value of the D_m term increases, and at T_f , a global minimum is generated at a finite m_a , and thus a first-order transition occurs. Hence in the region (ii), as temperature is lowered from T_s^+ , a second-order transition occurs firstly and then a first-order transition occurs as shown in Fig. 6(b) and (f).

Next, as $x \rightarrow x_e$, temperature T_s becomes T_f . Then, two global minima of $f(m_a)$ occur at $m_a = 0$ and $m_a > 0$, simultaneously. For this case, the second- and first-order transition lines are merged in the phase diagram. So this point is called critical endpoint as shown in Fig. 6(c) and (g). This type of PT is called a mixed-order transition. At this critical end point, the order parameter shows a sudden jump by the amount m_a . However, the susceptibility χ_m diverges at T_s^+ as it appears in a continuous PT.

Next, for $x_e < x < x_M$, the D_m term is large enough to generate a global minimum of $f(m_a)$ at a nonzero value m_a at T_f , which is higher than T_s . Then, only a discontinuous transition occurs at T_f as shown in Fig. 6(d) and (h).

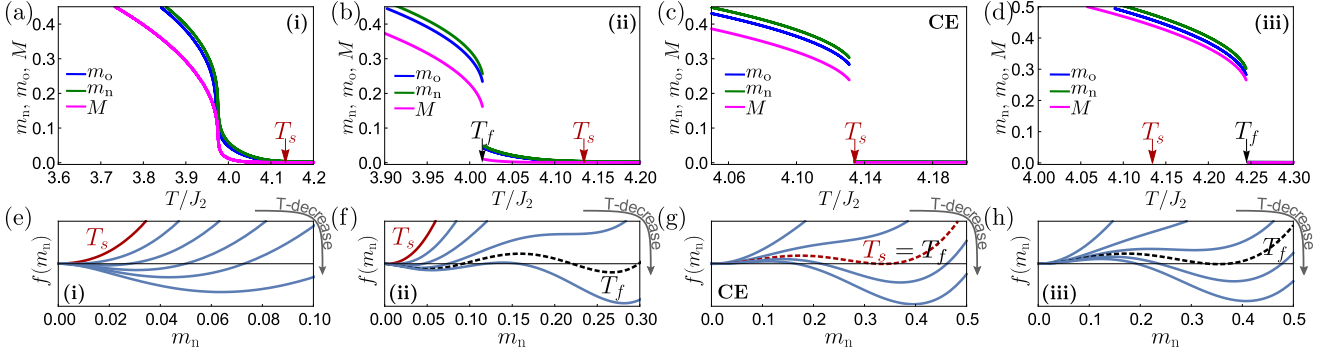


FIG. 6. (a)–(d) Plot of the order parameters m_a and M as a function of T/J_2 , and (e)–(h) Plot of the free energy landscapes as a function of m_n for $\lambda_n = 3.53$ and $\lambda_o = 3.90$ and various interlayer interaction ratios: $x = 1.30$ for (a) and (e); $x = 1.40$ for (b) and (f); $x = 1.62$ for (c) and (g); and $x = 1.80$ for (d) and (h). The transition types are second-order in region (i) (a) and (e); successive continuous-discontinuous in region (ii) for (b) and (f); mixed-order at CE_1 for (c) and (g); and discontinuous transition in region (iii) for (d) and (h).

B. When $x > x_M$

The self-consistency relations Eqs. (20) and (21) are expanded in terms of m_a and M as follows:

$$m_n \langle k_n \rangle \left(1 - K_2 \frac{\langle k_n^2 \rangle}{\langle k_n \rangle} \right) \simeq K_2 m_o \langle k_n \rangle \langle k_o \rangle - (\lambda_n - 1) C_n(\lambda_n) (K_2 m_n)^{\lambda_n - 2} + (K_4 M) (K_2 m_n) \langle k_n^2 \rangle \langle k_o \rangle + (K_4 M) (K_2 m_o) \langle k_n \rangle \langle k_o^2 \rangle + \text{h.o.} \quad (43)$$

$$m_o \langle k_o \rangle \left(1 - K_2 \frac{\langle k_o^2 \rangle}{\langle k_o \rangle} \right) \simeq K_2 m_n \langle k_n \rangle \langle k_o \rangle - (\lambda_o - 1) C_o(\lambda_o) (K_2 m_o)^{\lambda_o - 2} + D_M(\lambda_o) (K_4 M)^{\lambda_o - 3} (K_2 m_o) - \left[\int_0^1 dk_o P_d(k_o) \tanh(K_4 M k_o) k_o^2 \right] (K_2 m_o) + (K_4 M) (K_2 m_n) \langle k_n \rangle \langle k_o^2 \rangle + \text{h.o.} \quad (44)$$

$$M \langle k_o \rangle \left(1 - x K_2 \frac{\langle k_o^2 \rangle}{\langle k_o \rangle} \right) \simeq -(\lambda_o - 1) C_M(\lambda_o) (K_4 M)^{\lambda_o - 2} + (\lambda_o - 3) D_M(\lambda_o) (K_4 M)^{\lambda_o - 4} (K_2 m_o)^2 + \text{h.o.}, \quad (45)$$

where $D_M(\lambda_o) > 0$ increases monotonically with λ_o . This coefficient is explicitly derived in Appendix C. These expansions are valid for $3 < (\lambda_n, \lambda_o) < 4$ due to the power of the third term of the r.h.s of Eq. (44).

When $x > x_M$, $x \langle k_o^2 \rangle / \langle k_o \rangle > T_h$ and the l.h.s. of Eq (45) becomes negative for $T > T_h$. On the other hand, the first term of the r.h.s. of Eq. (45) is also negative; however, the second term is positive. So, the first term is comparable to the l.h.s., leading to $M \sim (T_{s,M}/T - 1)^{1/(\lambda_o - 3)}$, where $T_{s,M} \equiv x \langle k_o^2 \rangle / \langle k_o \rangle$. Thus, M exhibits a continuous transition at $T_{s,M}$, corresponding to the continuous transition curve starting from CE_2 in Fig. 3. Note that this formula is the same as the one

of the Ising model on a single SF network [2]. For further discussions, M_* is defined as

$$M_* \equiv \frac{1}{K_4} \left[\frac{\langle k_o \rangle (T_{s,M}/T - 1)}{(\lambda_o - 1) K_4 C_M(\lambda_o)} \right]^{1/(\lambda_o - 3)}.$$

Next, to determine a critical temperature (denoted as $T_{s,m}$) for m_a , we first rewrite Eq. (45) as

$$M \simeq M_* + \frac{D_M(\lambda_o)}{\langle k_o \rangle (T_{s,M}/T - 1)} (K_4 M_*)^{\lambda_o - 4} (K_2 m_o)^2 + \text{h.o.} \quad (46)$$

We consider the linear terms of m_a in Eqs. 43 and 44, and substitute M with M_* . Using a similar technique used in Eq. (33), we obtain the following:

$$\langle k_n \rangle \langle k_o \rangle \left(1 - \frac{\langle k_n^2 \rangle / \langle k_n \rangle + g_n(M_*)}{T} \right) \left(1 - \frac{\langle k_o^2 \rangle / \langle k_o \rangle + g_o(M_*)}{T} \right) - \left(\frac{\langle k_n \rangle \langle k_o \rangle}{T} + \frac{K_4 M_* \langle k_n \rangle \langle k_o^2 \rangle}{T} \right)^2 = 0, \quad (47)$$

where

$$g_n(M_*) \langle k_n \rangle = K_4 M_* \langle k_o \rangle \langle k_n^2 \rangle, \quad \text{and} \quad g_o(M_*) \langle k_o \rangle = D_M(\lambda_o)(K_4 M_*)^{\lambda_o-3} - \int_0^1 dk_o P_d(k_o) \tanh(K_4 M_* k_o) k_o^2.$$

Eq. (47) has two solutions for T , denoted as T'_ℓ and T'_h ($T'_\ell < T'_h$). Using the relation (46), we obtain a self-consistency relation for m_a within the leading order as follows:

$$m_a \langle k_o \rangle \langle k_n \rangle \left(1 - \frac{T'_\ell}{T} \right) \left(1 - \frac{T'_h}{T} \right) \simeq -(\lambda_a - 1) E'_a C_a(\lambda_a) (K_2 m_a)^{\lambda_a-2} - (\lambda_{\bar{a}} - 1) F'_{a\bar{a}} C_{\bar{a}}(\lambda_{\bar{a}}) (K_2 m_{\bar{a}})^{\lambda_{\bar{a}}-2}, \quad (48)$$

where $E'_a = \langle k_{\bar{a}} \rangle \left(1 - \frac{\langle k_{\bar{a}}^2 \rangle / \langle k_{\bar{a}} \rangle + g_{\bar{a}}(M_*)}{T} \right)$ and $F'_{a\bar{a}} = \frac{1}{T} \langle k_o \rangle \langle k_n \rangle + \frac{1}{T} K_4 M_* \langle k_o^2 \rangle \langle k_n \rangle$. We find that near T'_h , m_a converges to zero continuously, whereas M remains in $O(1)$. Hence, we regard T'_h as the critical temperature T'_s of m_a . Note that M has the critical temperature $T_{s,M}$ separately, given as $x \langle k_o^2 \rangle / \langle k_o \rangle$, which is higher than T'_s .

Using Eq. (46), we expand the free energy density of Eq. (17) with respect to m_a up to the three lowest order terms:

(i) For $\lambda_n > \lambda_o$,

$$f(m_o) \simeq f_0(M_*) + A'_0 K_2 m_o^2 \left(1 - \frac{T'_s}{T} \right) + C_o(\lambda_o) (K_2 m_o)^{\lambda_o-1} + C_n(\lambda_n) (B'_0 m_o)^{\lambda_n-1} \\ - \frac{K_2 [(\lambda_n - 1) C_n(\lambda_n)]^2}{\langle k_n \rangle \left[1 - \left(\langle k_n^2 \rangle / \langle k_n \rangle + g_n(M_*) \right) / T \right]} (B'_0 m_o)^{2(\lambda_n-2)} - \frac{1}{2} (\lambda_o - 3) \frac{K_4 [D_M(\lambda_o) (K_4 M_*)^{\lambda_o-4}]^2}{\langle k_o \rangle (T_{s,M}/T - 1)} (K_2 m_o)^4 + \text{h.o.}, \quad (49)$$

where A'_0 and B'_0 are functions of λ_a , K_2 and $K_4 M_*$. They are explicitly derived in Appendix D.

(ii) For $\lambda_n < \lambda_o$,

$$f(m_n) \simeq f_0(M_*) + A'_n K_2 m_n^2 \left(1 - \frac{T'_s}{T} \right) + C_n(\lambda_n) (K_2 m_n)^{\lambda_n-1} + C_o(\lambda_o) (B'_n m_n)^{\lambda_o-1} \\ - \frac{K_2 [(\lambda_o - 1) C_o(\lambda_o)]^2}{\langle k_o \rangle \left[1 - \left(\langle k_o^2 \rangle / \langle k_o \rangle + g_o(M_*) \right) / T \right]} (B'_n m_n)^{2(\lambda_o-2)} - \frac{1}{2} (\lambda_o - 3) \frac{K_4 [D_M(\lambda_o) (K_4 M_*)^{\lambda_o-4}]^2}{\langle k_o \rangle (T_{s,M}/T - 1)} (B'_n m_n)^4 + \text{h.o.}, \quad (50)$$

where A'_n and B'_n are functions of λ_a , K_2 and $K_4 M_*$. They are explicitly derived in Appendix D. Here, first two C_a terms are positive, like the case $x < x_M$,

The first two C_a terms in Eqs.(49) and (50) are positive, as for the case $x < x_M$, whereas the next two terms containing C_a and D_M are negative. The $2(\lambda_a - 2)$ -order terms with C_a are finite, whereas the D_M term diverges as $T \rightarrow T_{s,M}$. Thus, the D_M term contributes to the formation of a global minimum of $f(m_a)$ as T is decreased T_f and $x \rightarrow x_M^+$.

We also consider the case of $\lambda_n = 3.53$ and $\lambda_o = 3.90$.

Firstly, as $x \rightarrow \infty$ in the region (vi), the D_M terms are too small, the global minima of $f(m_a)$ and $f(M)$ occur at $m_a = 0$ and $M = 0$ for $T > T_{s,M}$, respectively. M and m_a exhibit second-order transitions at $T_{s,M}$ and T'_s , respectively. A first-order transition does not occur. These behaviors are schematically shown in Fig. 7 (d) and (h).

Using Eqs. (49) and (50), it is obtained that m_a and M be-

have as

$$m_a \sim (T'_s - T)^{\beta_m} \quad \text{with} \quad \beta_m = \frac{1}{\lambda_{\min} - 3}, \quad (51)$$

$$M \sim (T_{s,M} - T)^{\beta_M} \quad \text{with} \quad \beta_M = \frac{1}{\lambda_o - 3}, \quad (52)$$

where $\lambda_{\min} = \min(\lambda_o, \lambda_n)$. Using these results, we obtain the specific heats, which behave as

$$C_m \sim (T'_s - T)^{-\alpha_m} \quad \text{with} \quad \alpha_m = \frac{\lambda_{\min} - 5}{\lambda_{\min} - 3}, \quad (53)$$

$$C_M \sim (T_{s,M} - T)^{-\alpha_M} \quad \text{with} \quad \alpha_M = \frac{\lambda_o - 5}{\lambda_o - 3}. \quad (54)$$

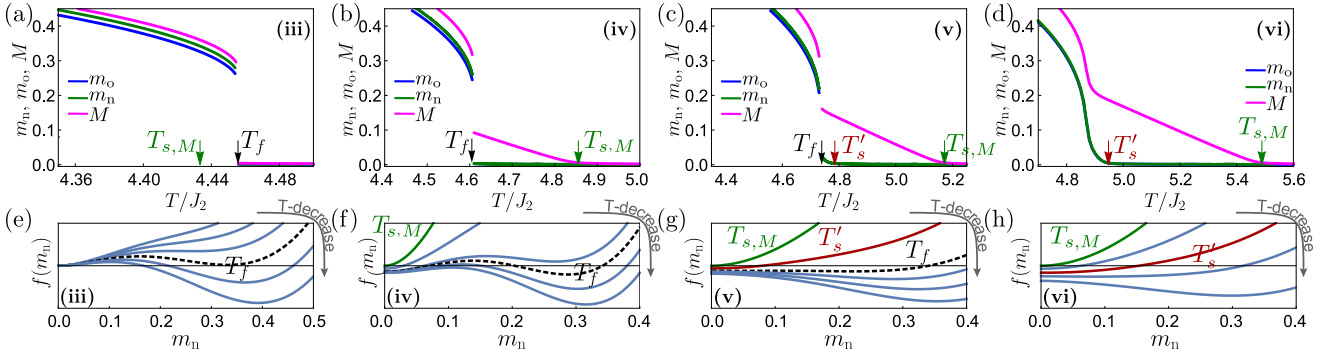


FIG. 7. (a)–(d) Plot of the order parameters m_a and M as a function of T/J_2 . (e)–(h) Plot of the free energy landscapes as a function of m_n for $\lambda_n = 3.53$ and $\lambda_o = 3.90$ and various interlayer interaction ratios: $x = 2.10$ for (a) and (e); $x = 2.30$ for (b) and (f); $x = 2.45$ for (c) and (g); and $x = 2.60$ for (d) and (h). The transition types are first-order in regime (iii) for (a) and (e); successive continuous-discontinuous in regime (iv) for (b) and (f); successive continuous-discontinuous in regime (v) for (c) and (g); and continuous transition in regime (vi) for (d) and (h).

The susceptibilities behave as follows:

$$\chi_m \sim \begin{cases} (T - T'_s)^{-\gamma_m^+} & \text{with } \gamma_m^+ = 1, \\ (T'_s - T)^{-\gamma_m^-} & \text{with } \gamma_m^- = 1, \end{cases} \quad (55)$$

and

$$\chi_M \sim \begin{cases} (T - T_{s,M})^{-\gamma_M^+} & \text{with } \gamma_M^+ = 1, \\ (T_{s,M} - T)^{-\gamma_M^-} & \text{with } \gamma_M^- = 1. \end{cases} \quad (56)$$

Detailed derivations of χ_M and χ_m near $T_{s,M}$ and T'_s , respectively, are given in Appendix E.

Secondly, in the region (v), when $T > T_{s,M}$, the D_M terms are too small, and the global minima of $f(m_a)$ and $f(M)$ remain at $m_a = 0$ and $M = 0$, respectively. For $T'_s < T < T_{s,M}$, the global minimum of $f(M)$ occurs at a finite M , which increases continuously as T is lowered gradually. Meanwhile, the global minimum of $f(m_a)$ remains at still $m_a = 0$. As T is lowered across T'_s , the global minimum of $f(m_a)$ emerges at a finite $m_a > 0$. Thus, m_a is finite, and a second-order transition occurs at T'_s . M increases continuously. When T is somewhat lowered and reaches T_f , the global minima of $f(m_a)$ and $f(M)$ occur at finite m_a and M , separated from the respective positions at T_f^+ . Thus, first-order transitions occur at T_f . These behaviours are schematically shown in Fig. 7 (c) and (g).

Next, at the boundary between the regions (v) and (iv), denoted as CE₃, the magnetization m_a changes discontinuously from 0 to a finite value at T_s^- ; however, the susceptibility χ_m diverges at T_s^{++} . Thus, a mixed-order PT appears at CE₃.

Next, in the region (iv), the D_M terms are not large in magnitude, so that the global minima of $f(m)$ and $f(M)$ remain at $m = 0$ and $M = 0$, respectively. For $T < T_{s,M}$, a global minimum of $f(M)$ appears at finite $M > 0$, which increases continuously as T is lowered. As T is decreased further, the D_M terms increase. When T reaches T_f , new global minima of $f(m_a)$ and $f(M)$ appear at certain finite m_a and M far from values at T_f^+ , respectively. Thus, a first-order transition appears for each m_a and M , respectively. Hence in the region (iv), as T is lowered from $T_{s,M}^+$, a continuous transition occurs for M firstly and then first-order transitions occur for each m_a and M . These behaviors are shown in Fig. 7 (b) and (f).

Next, at the boundary between the regions (iv) and (iii), denoted as CE₂ in Fig. 3, M drops to 0 from a finite value at $T_{s,M}^-$, and thus the susceptibility does not diverge. However, when T approaches $T_{s,M}^+$, even though M jumps suddenly and shows a behavior of the first-order transition, the susceptibility χ_M diverges. This is due to the presence of the second-order transition curve of M along the boundary between $\langle \sigma s \rangle$ and paramagnetic phases. Thus, the magnetization of M exhibits the properties of a mixed-order transition.

Next, in the region (iii), the D_M term diverges as $T \rightarrow T_{s,M}$. Thus, the D_M term is large enough to generate a global minima of $f(m_a)$ and $f(M)$ as T is decreased to T_f . Those T_f are higher than $T_{s,M}$. Then, discontinuous transitions occur for m_a and M at T_f . These behaviors are shown in Figs. 7(a) and (e).

TABLE I. Critical exponents for $3 < (\lambda_n, \lambda_o) < 4$.

Range of x	α_m	α_M	β_m	β_M	$\gamma_{m\pm}$	$\gamma_{M\pm}$
$x = 0$	$\frac{\lambda_{\min}-5}{\lambda_{\min}-3}$	-	$\frac{1}{\lambda_{\min}-3}$	-	1	-
$x = x_M$ ($\lambda_n > \lambda_o$)	$\frac{\lambda_o-5}{\lambda_o-3}$	$\frac{\lambda_o-5}{\lambda_o-3}$	$\frac{1}{\lambda_o-3}$	$\frac{1}{\lambda_o-3}$	1	0
$x = x_M$ ($\lambda_n < \lambda_o$)	$\frac{\lambda_n-5}{\lambda_n-3}$	$\frac{\lambda_o-5}{\lambda_o-3}$	$\frac{1}{\lambda_n-3}$	$\frac{1}{\lambda_o-3}$	1	1
$0 < x < x_M$	$\frac{\lambda_{\min}-5}{\lambda_{\min}-3}$	$\frac{\lambda_{\min}-5}{\lambda_{\min}-3}$	$\frac{1}{\lambda_{\min}-3}$	$\frac{\lambda_o-2}{\lambda_o-3}$	1	0
$x > x_M$ (region (iv))	$\frac{\lambda_{\min}-5}{\lambda_{\min}-3}$	$\frac{\lambda_o-5}{\lambda_o-3}$	$\frac{1}{\lambda_{\min}-3}$	$\frac{1}{\lambda_o-3}$	1	1

C. Sensitivity of PTs to λ_n and λ_o around x_M^\pm

In the previous two subsections, we showed that as $x \rightarrow x_M^\pm$ for a fixed set of $\lambda_n = 3.53$ and $\lambda_o = 3.90$, the transition types become more complicated. Here, we also show that types of PTs are sensitive to λ_n and λ_o as $x \rightarrow x_M^\pm$. When λ_n and λ_o are decreased but with a fixed x near x_M , the C_n and C_o terms increase, respectively. As a consequence, the magnitudes of the D_m and D_M terms decrease compared to those of the C_n and

C_0 terms. The system exhibits a second-order transition at a transition temperature T_s around x_M . A new global minimum by the D_m and D_M terms occurs at a lower temperature.

When λ_0 is fixed as 3.90 but λ_n is decreased to 3.35, then the magnitudes of the D_m and D_M terms become comparable to those of the C_n and C_0 terms at a lower temperature, denoted as T_f , lower than T_s at given x around x_M . The discontinuous transition curve are separated from the second-order transition line as shown in Fig. 5(b). If λ_n are decreased further to 3.30, the magnitudes of D_M terms become much smaller than those of the C_a terms, so the system does not generate a global minimum at any T for $x > x_M$; whereas the D_m term make a global minimum of the free energy density at $T_f < T_s$ for $x < x_M$. Thus a discontinuous transition curve appears only in the l.h.s. of the phase diagram as shown in Fig. 5(a).

When λ_n is fixed as 3.53 but λ_0 is decreased lower than 3.50 ($< \lambda_c$), the D_m and D_M terms make discontinuous transitions only for $T_f < T_s$ at given x around x_M . Thus, a discontinuous transition curve appears at T_f , separated from the second-order curve as shown in Fig. 5(e). If λ_0 are further decreased to 3.30, the magnitudes of D_m and D_M terms becomes smaller, so the D_m and D_M terms do not produce a global minimum for all x and thus a discontinuous transition curve does not appear in the phase diagram as shown in Fig. 5(d).

When λ_n is fixed as 3.53 ($> \lambda_c$) but λ_0 is changed but still larger than λ_c , two discontinuous transition curves appear in the phase diagram as shown in Fig. 5(f). Detailed discussions are presented in the following Sec V.

D. Anomalous Scaling Relations

The critical exponents of the continuous transition are listed in Table I for all ranges of x . Here, α is the exponent of specific heat, β_m (β_M) is the exponent of the magnetization m_a (M) at zero external magnetic field, and γ_m (γ_M) is the exponent of susceptibility for m_a (M)-magnetization near a transition temperature.

The scaling relation for m_a satisfies the conventional relation:

$$\alpha + 2\beta_m + \gamma_m = 2. \quad (57)$$

By contrast, the scaling relation for M shows unusual behavior for $x < x_M$. The susceptibility exponent γ_M is 0. Thus, the scaling relation for M does not hold for $x < x_M$ as

$$\alpha + 2\beta_M + \gamma_M = \begin{cases} 3 & \text{for } \lambda_n > \lambda_0, \\ 3 + 2\frac{\lambda_0 - \lambda_n}{\lambda_n - 3} & \text{for } \lambda_n < \lambda_0. \end{cases} \quad (58)$$

Note that for the original AT model, the scaling relation for M is written as $\alpha + 2\beta_M + \gamma_M = 3$. This relation can be confirmed by setting $\lambda_n = \lambda_0$ in the second equation of (58).

VI. PHASE TRANSITIONS AROUND x_M

In previous section, we have described the continuous transitions for both $x \rightarrow 0$ and $x \gg x_M$ cases, in which the magnitude of the D_m (D_M) term of $f(m_a)$ is negligible compared with the C_a term. However, as $x \rightarrow x_M^-$ ($x \rightarrow x_M^+$) and $T \rightarrow T_s$ ($T'_s = T_{s,M}$), the D_m (D_M) term is increased, and becomes large enough, so that they cannot be ignored compared to the C_a terms. Then another global minimum of $f(m_a)$ can be generated by the D_m (D_M) term as $x \rightarrow x_M^-$ ($x \rightarrow x_M^+$), depending on the degree exponents λ_n and λ_0 .

Thus, a phase diagram is mainly determined by a type of PT at $x = x_M$. If a discontinuous transition occurs at $x = x_M$, then diverse types of PTs appear depending on x . Otherwise, only continuous transitions occur for all x as shown in Fig. 5(d), except some special cases that discontinuous transitions occur for $x < x_M$ as shown in Fig. 5(a). Below we discuss the type of PT at $x = x_M$ depending on the degree exponents (λ_n, λ_0) .

A. When $\lambda_n \geq \lambda_0$

In this case, $O(m_a) \sim O(M)$ near T_s and the free energy density of Eq. (17) is expanded with respect to m_0 as follows:

$$f(m_0) \simeq A_0 K_2 m_0^2 \left(1 - \frac{T_s}{T}\right) + \frac{1}{2} K_4 M^2 \langle k_0 \rangle \left(1 - \frac{T_s}{T}\right) + C_0(\lambda_0, r_0) (K_2 m_0)^{\lambda_0 - 1} + C_n(\lambda_n) (B_0 m_0)^{\lambda_n - 1} + C_3(\lambda_n, \lambda_0, r_0) (K_2 m_0)^3 + \text{h.o.}, \quad (59)$$

where A_0 and B_0 are functions of λ_a and K_2 that are explicitly derived in Appendix D. $C_0(\lambda_0, r_0)$ with $r_0 \equiv K_4 M / K_2 m_0$ is $O(1)$. Explicit formulas of the coefficients are given in Appendices C and D, respectively.

We note that the C_0 term is a leading order term at T_s , and C_0 decreases monotonically with λ_0 . Thus the sign of C_0 can change depending on the magnitude of λ_0 . This feature does not appear for both $0 < x < x_M$ and $x > x_M$ cases. However, it occurs when $x = x_M$. Numerically $C_0 = 0$ at $\lambda_0 \approx 3.503$,

equivalent to λ_c introduced earlier in Secs. II and III: C_0 becomes positive for $\lambda_0 < \lambda_c$, whereas it is negative for $\lambda_0 > \lambda_c$. On the other hand, C_n and C_3 are always positive and negative, respectively.

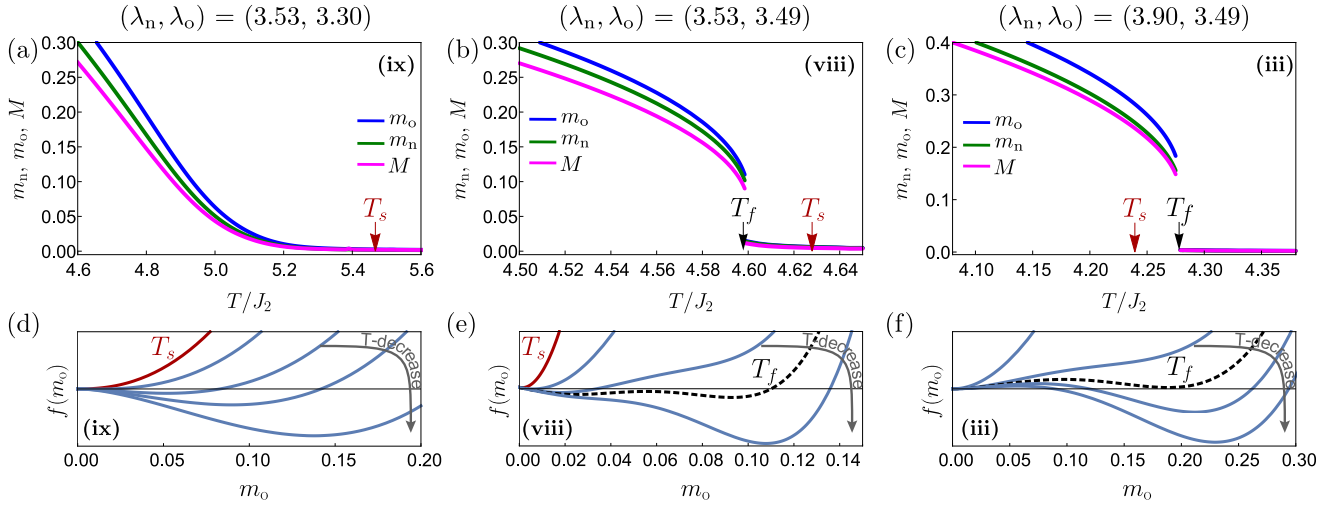


FIG. 8. (a)–(c) Plots of the order parameters m_a and M at $x = x_M$ as a function of T . (d)–(f) Plots of the free energy landscapes as a function of m_o for various T . The degree exponents taken for (a) and (d) are $(\lambda_n, \lambda_o) = (3.53, 3.30)$; for (b) and (e) are $(3.53, 3.49)$; and for (c) and (f) are $(3.90, 3.49)$. For comparison, note that $\lambda_c \approx 3.503$

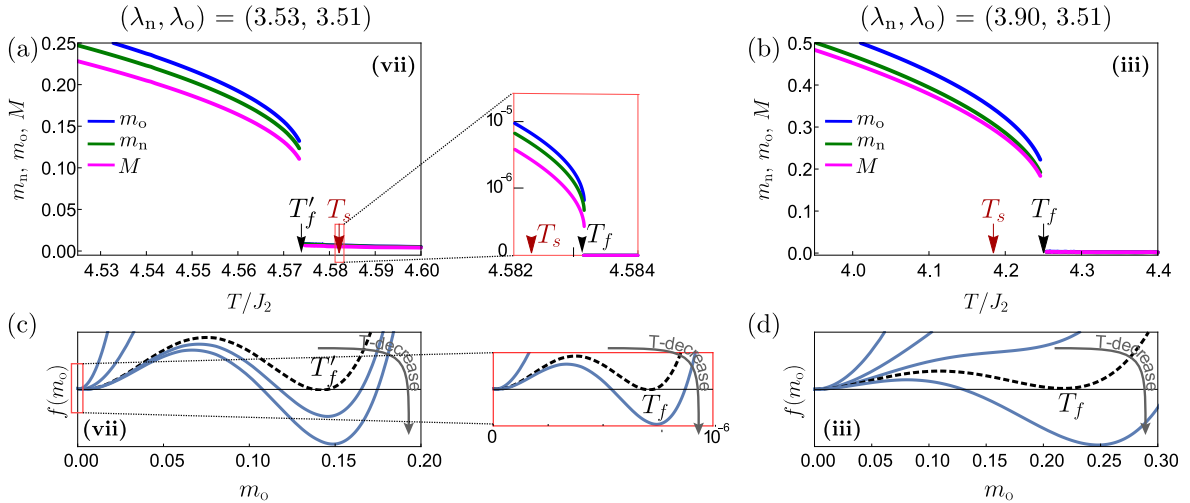


FIG. 9. (a) and (b) Plots of the order parameters m_a and M at $x = x_M$ as a function of T/J_2 . (c) and (d) Plots of the free energy landscapes as a function of m_o for the temperatures around T_f . The degree exponents for (a) and (c) are taken as $(\lambda_n, \lambda_o) = (3.53, 3.51)$ and for (b) and (d) are taken as $(3.90, 3.51)$.

I. For $\lambda_o < \lambda_c$

When $\lambda_o < \lambda_c$, for instance $\lambda_o \approx 3$, the C_o term is positive and large enough compared to the C_3 term. Thus, a global minimum of $f(m_o)$ remains at $m_a = M = 0$ for $T \geq T_s$ and emerges continuously at finite values m_a and M as T is decreased from T_s^- , respectively. At T_s , thus, m_a and M exhibit continuous PTs. This type of PT occurs in the region (ix) in Fig. 4(b). The order parameters and free energy configurations are depicted in Fig. 8 (a) and (d), respectively. This continuous transitions look the same as that of the (i)-type PTs; however, the critical behavior for M of this continuous transition differs from that of the (i)-type PT, and thus we denote this type of a continuous transition as a (ix)-type PT to distinguish this from the (i)-type PTs.

Using Eqs. (59), it is obtained that the magnetizations behave as

$$m_a \sim (T_s - T)^{\beta_m} \quad \text{with} \quad \beta_m = \frac{1}{\lambda_o - 3}, \quad (60)$$

$$M \sim (T_s - T)^{\beta_M} \quad \text{with} \quad \beta_M = \frac{1}{\lambda_o - 3}, \quad (61)$$

The specific heat behaves as

$$C \sim (T_s - T)^{-\alpha} \quad \text{with} \quad \alpha = \frac{\lambda_o - 5}{\lambda_o - 3}. \quad (62)$$

The susceptibilities behave as follows:

$$\chi_m \sim \begin{cases} (T - T_s)^{-\gamma_m^+} & \text{with } \gamma_m^+ = 1, \\ (T_s - T)^{-\gamma_m^-} & \text{with } \gamma_m^- = 1, \end{cases} \quad (63)$$

and

$$\chi_M \sim \begin{cases} (T - T_s)^{-\gamma_M^+} & \text{with } \gamma_M^+ = 1, \\ (T_s - T)^{-\gamma_M^-} & \text{with } \gamma_M^- = 1. \end{cases} \quad (64)$$

The derivation of χ_a is presented in Appendix E. Note that the β_M and χ_M of the (ix)-type PTs are different from those of the (i)-type PTs.

As λ_o approaches λ_c^- , then C_o decreases. For $T > T_s$, the C_3 term is still small to generate a global minimum. Thus, the global minimum of $f(m_o)$ remains at $m_a = M = 0$. However, as T is further lowered below a certain temperature T_f , the C_3 term becomes large enough to generate a global minimum at a certain $m_a > 0$, and a discontinuous transition occurs. Thus, as T is decreased from T_s^+ , a continuous transition occurs firstly at T_s , followed by a discontinuous transition at T_f . This type of PTs occur in the region (ii) in Fig. 4(b). The order parameters and free energy configurations are depicted in Fig. 8 (b) and (e), respectively.

When λ_n is set as 4 large enough but λ_o is still around λ_c^- , C_n decreases. Then, the C_3 term is large enough to produce a global minimum of $f(m_o)$ at a certain temperature T_f higher than T_s . For this case, a discontinuous transition occurs at T_f . This type of PT occurs in the region (iii) in Fig. 4(b). The order parameters and free energy configurations are depicted in Fig. 8 (c) and (f), respectively.

2. For $\lambda_o > \lambda_c$

When both λ_n and λ_o are close to λ_c^+ , the C_o term becomes negative. Thus, a global minimum of $f(m_o)$ is generated at a certain T_f higher than T_s and then a discontinuous PT occurs at T_f . As T is further lowered from T_f , the global minimum position of m_a and M increases continuously until a certain T_f' lower than T_s . When T reaches T_f' , another global minimum of $f(m_o)$ is generated by the C_3 term. This minimum position

of m_a is far away from the global minimum produced at T_f . This means that another first-order transition occurs. Therefore, two successive discontinuous transitions occur, which are mainly contributed by the C_o term at T_f , and the competition between the C_n and C_3 terms at T_f' , respectively. This type of PTs occur in the region (vii) in Fig. 4(b). The order parameters and free energy configurations are depicted in Fig. 9 (a) and (c), respectively.

When λ_n is increased to 4 and λ_o is around λ_c^+ , the C_n term decreases. Thus, two different local minima of $f(m_o)$, generated by the C_o term and the competition between C_3 and C_n terms, respectively, are merged into one giant local minimum. A global minimum of $f(m_o)$ is generated by C_o and C_3 terms at a certain temperature T_f higher than T_s . Then, a discontinuous PT occurs at T_f . The order parameters and free energy configurations are depicted in Figs. 9(b) and (d).

B. When $\lambda_n = \lambda_o$

When $\lambda_n = \lambda_o$, the C_o and C_n terms in Eq. (59) are of the same order. Thus, the two terms are combined and denoted as $C'_o(\lambda_o, r_o)(K_2 m_o)^{\lambda_o-1}$. The sign of C'_o depends on λ_o , equivalently λ_n . Numerically C'_o can be zero at a certain λ_o , denoted as λ_e , estimated to be ≈ 3.605 . C'_o becomes positive for $\lambda_o < \lambda_e$ and negative otherwise.

Similar to the previous case $\lambda_n > \lambda_o$, a discontinuous transition always occurs for $C'_o < 0$. However, depending on relative magnitude between two terms C'_o and C_3 , either a discontinuous or continuous transition occurs for $C'_o > 0$. Note that successive discontinuous transitions do not occur for $\lambda_n = \lambda_o$.

C. When $\lambda_n < \lambda_o$

When $\lambda_n < \lambda_o$, $O(m_a) \ll O(M)$, the free energy density of Eq. (17) is expanded with respect to m_n as follows:

$$f(m_n) \simeq f_0(M_*) + A'_n K_2 m_n^2 \left(1 - \frac{T_s}{T}\right) + C_n(\lambda_n)(K_2 m_n)^{\lambda_n-1} + C_o(\lambda_o)(B'_n m_n)^{\lambda_o-1} \\ - \frac{K_2[(\lambda_o - 1)C_o(\lambda_n)]^2}{\langle k_o \rangle \left[1 - (\langle k_o^2 \rangle / \langle k_o \rangle + g_o(M_*)) / T\right]} (B'_n m_n)^{2(\lambda_o-2)} - \frac{1}{2}(\lambda_o - 3) \frac{K_4 [D_M(\lambda_o)(K_4 M_*)^{\lambda_o-4}]^2}{\langle k_o \rangle (T_{s,M}/T - 1)} (B'_n m_n)^4 + \text{h.o.},$$

This formula is exactly the same as Eq. (50), derived in Sec.IV (B) for continuous transitions. For this case, the three types of domains (iii), (v), and (vi) exist in the phase diagram shown in Fig. 4(b). We remark that the critical exponents for m_a and M are obtained as the same as those of (iv)-type PTs, respectively. However, the transition temperatures T_s' and $T_{s,M}$ are the same, so that they reduce to T_s .

When λ_n small enough, for instance about 3.3, the C_n term is large enough compared to the D_M term. Thus, a global min-

imum of $f(m_n)$ remains at $m_a = M = 0$ for $T \geq T_s$, and emerges at finite m_a and M as T is decreased from T_s . At T_s , m_a and M exhibit continuous PTs. These behaviors are schematically shown in Fig. 10(a) and (d).

When λ_n is increased to λ_c^- , C_n decreases. For $T > T_s$, the D_M term is not large enough to generate a global minimum, the global minimum of $f(m_n)$ remains at $m_a = M = 0$. When T is lower than T_s , a continuous transition occurs. As T is further lower than a T_f , the D_M term becomes large enough

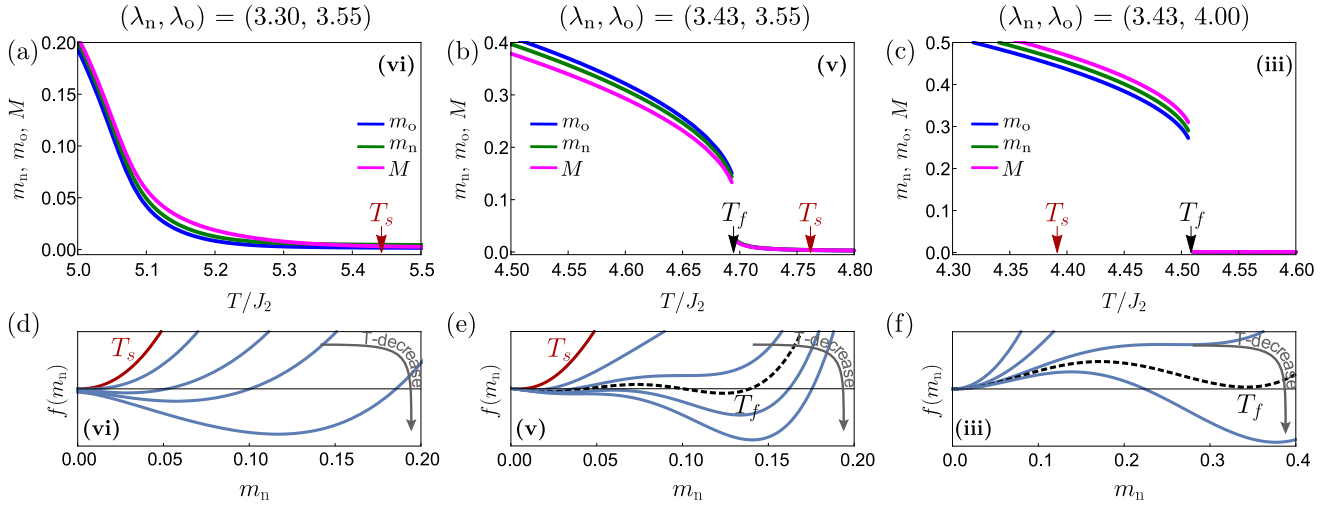


FIG. 10. (a)–(c) Plots of the order parameters m_a and M at $x = x_M$ as a function of T/J_2 . (d)–(f) Plots of the free energy landscapes as a function of m_n for various T . The degree exponents taken for (a) and (d) are $(\lambda_n, \lambda_o) = (3.30, 3.55)$; for (b) and (e) are $(3.43, 3.55)$; and for (c) and (f) are $(3.43, 4.00)$.

to generate a new global minimum at the position far from the previous position of the continuous transition. Thus, as T is decreased from T_s^+ , a continuous PT occurs at T_s firstly and then a discontinuous PT occurs at T_f as shown in Fig. 10(b) and (e).

When λ_n is around λ_c^- and λ_o is increased to 4, C_o decreases. The D_M term is large enough to produce a global minimum of $f(m_n)$ at a certain T_f higher than T_s . Then, a discontinuous PT occurs at T_f . These behaviors are shown in Figs. 10(c) and (f).

VII. DISCUSSION

Here, we recall three previous results: (i) The maximum degree of an SF network with degree exponent λ is given as $k_{\max} \sim N^{1/(\lambda-1)}$ in a finite system of size N . Thus, as λ increases, the maximum degree k_{\max} of the SF network decreases. (ii) The Ising model on an SF network with degree exponent λ exhibits a PT at temperature $T_c \propto (\lambda - 2)/(\lambda - 3)$ for $\lambda > 3$. Thus, as λ increases, T_c decreases. Therefore, because the magnetization corresponds to the opinion formed, it is likely that the degree of a hub may represent the strength of opinion formation [39]. (iii) For the original AT model, when $x = J_4/J_2 = 1$, the model is reduced to the Potts model with four states. Then, there exists a critical degree exponent $\lambda_c \approx 3.503$ such that for $\lambda_o > \lambda_c$, the PT is of the first-order; otherwise, it is of the second-order [40].

The g -AT model may be regarded as a combination of the original AT model on the network of overlapping links and two independent Ising models on the respective network of non-overlapping links. Depending on the degree exponents of the two networks of overlapping and non-overlapping links, three cases occur: (i) If the strength of a common opinion formation by an overlapping network, mainly contributed by the interlayer J_4 -interaction, is not sufficiently strong, then two independent Ising models on the network comprising non-

overlapping and overlapping links with the J_2 -interaction are considered to be effective. Thus, opinions were formed for each spin community. (ii) Conversely, if the strength is sufficiently strong, a common opinion is formed on the overlapping network, realized by the non-zero magnetization of the σ_s spin. (iii) In the intermediate range between the above-mentioned two conditions, intralayer and interlayer interactions are in conflict, generating a first-order transition and rich phase diagrams. The strengths of the interlayer and intralayer interactions are determined not only by the ratio J_4/J_2 but also by λ_n , λ_o , and λ_c .

First, we consider the case of $\lambda_n > \lambda_o$ and $\lambda_o < \lambda_c$ (Fig. 8). When $\lambda_n = 3.53$ and $\lambda_o = 3.30$ in (a), the hub strengths of both the overlapping and non-overlapping networks are sufficiently large, and thus, opinions are formed smoothly at a high temperature $T_c \approx 5.45$. When λ_o is increased to 3.49 in (b), the hub strength of the overlapping network is weakened. Therefore, at a relatively lower temperature $T_c \approx 4.63$, opinions are formed separately in each spin community. As the temperature decreases further (e.g., $T_c \approx 4.6$), a common opinion is formed through the J_4 -interaction by overcoming the suppression of the overlapping and non-overlapping links by the hubs. Thus, the transition is of the first-order. (c) When λ_n is increased to 3.90, the hub strength of the non-overlapping network for the opinion formation of each community is also weakened. Thus, a first-order transition occurs because of the conflict between the hubs of the non-overlapping and overlapping networks and the interlayer J_4 -interaction.

Next, let us consider the case of $\lambda_n < \lambda_o$ and $\lambda_o > \lambda_c$ (Fig. 10). When $\lambda_n = 3.30$ and $\lambda_o = 3.55$, the hub strengths of the non-overlapping and overlapping networks are sufficiently strong, and thus, they form opinions gradually at $T_s \approx 5.45$, as depicted in Fig. 10(a). When λ_n is increased to 3.43 in (b), the hub strength of the non-overlapping network is weakened. Thus, opinions are formed in each community first at $T_s \approx 4.76$. As the temperature is lowered, a common opinion

is formed at $T_f \approx 4.69$; however, this formation is the consequence of overcoming the suppression of the overlapping and non-overlapping links by the hubs. Thus, the transition is of the first-order. When λ_o is increased to 4.00 in (c), the hub strength of the overlapping network is weakened. Because the strengths of both hubs are weak, the system exhibits a first-order transition, as illustrated in Fig. 10(c).

VIII. SUMMARY

To investigate the effect of link overlap on the dynamics of opinion formation defined on a multiplex network, we studied the so-called g -AT model, a spin model in equilibrium systems. The g -AT model describes the dynamics of two species of Ising spins, namely the s and σ spins, each of which is located on a single layer of the duplex network under consideration. Here, the model is defined on duplex networks with an SF multidegree distribution, which facilitates tuning of the effect of overlapping links with respect to non-overlapping links. In particular, we distinguish between multilinks (1, 1) that characterize overlapping links and multilinks (1, 0) and (0, 1) that do not. We assume that the multidegrees $k^{(1,1)} = k_o$ and $k^{(1,0)} = k^{(0,1)} = k_n$ follow power-law distributions associated with the tunable power-law exponents λ_n and λ_o . This system is illustrated in Fig. 1.

Pairs of s -spins (pairs of σ -spins) connected by overlapping

and non-overlapping links interact through a 2-body interaction of strength J_2 . Four spins comprising two s -spins and two σ -spins connected by overlapping links interact through a 4-body interaction with strength J_4 (see Fig. 2). The ratio $x \equiv J_4/J_2$ is a control parameter that can alter the critical properties of the model, and the system is assumed to be in thermal contact with the temperature T . Thus, there exist four control parameters, namely λ_n , λ_o , x , and T . By applying the Landau–Ginzburg theory, we obtained rich phase diagrams in the four-parameter space. The g -AT model is a generalization of the original AT model [37], in which all the links are regarded as overlapping links; therefore, a single exponent λ_o is considered in this context.

We note that the different species of spins represent individuals from two different communities formed based on friendship and business relations, respectively. Each pair of individuals may be connected solely via friendship links, solely via business relations, or via both relationships. An opinion formed is represented by the magnetizations $\langle \sigma \rangle$, $\langle s \rangle$, and $\langle \sigma s \rangle$ in the spin model, which can be accomplished through non-overlapping or overlapping links. The diversity of individual opinions is reflected by thermal fluctuations.

We investigated PTs arising from the competition between the opinion formation of each community and that of the entire society, and obtained rich phase diagrams including diverse types of PTs. These findings are expected to be beneficial in understanding the underlying mechanisms of local and global opinion formation in a society.

Appendix A: Self-consistency equation with an external magnetic field

With the external magnetic field

$$\Omega_a \equiv K_2 m_a + H_a, \quad \text{and} \quad \Omega_M \equiv K_4 M + H_4, \quad (\text{A1})$$

the self-consistency equations Eqs. (23) for m^a and M of the g -AT model are replaced as follows:

$$m_a \langle k_a \rangle = m_{a1} \equiv \int_{k_{\min}^n}^{\infty} \int_{k_{\min}^o}^{\infty} dk_n dk_o P_d(k_n) P_d(k_o) \frac{\tanh(\Omega_o k_o + \Omega_n k_n) [1 + \tanh(\Omega_4 k_o)]}{1 + \tanh^2(\Omega_o k_o + \Omega_n k_n) \tanh(\Omega_4 k_o)} k_a \quad (\text{A2})$$

and

$$M \langle k_o \rangle = M_1 \equiv \int_{k_{\min}^n}^{\infty} \int_{k_{\min}^o}^{\infty} dk_n dk_o P_d(k_n) P_d(k_o) \frac{\tanh(\Omega_4 k_o) + \tanh^2(\Omega_o k_o + \Omega_n k_n)}{1 + \tanh^2(\Omega_o k_o + \Omega_n k_n) \tanh(\Omega_4 k_o)} k_o. \quad (\text{A3})$$

Appendix B: Definitions of the \mathcal{A} terms in exact susceptibility formula

The \mathcal{A} terms are defined as follows:

$$\mathcal{A}_{aa} = \int_{k_{\min}^n}^{\infty} \int_{k_{\min}^o}^{\infty} dk_n dk_o P_d(k_n) P_d(k_o) \frac{(1 - \mathcal{T}_2^2 \mathcal{T}_4)(1 + \mathcal{T}_4)}{(1 + \mathcal{T}_2^2 \mathcal{T}_4)^2 \cosh^2(K_2(m_o k_o + m_n k_n))} k_a^2, \quad (\text{B1})$$

$$\mathcal{A}_{a\bar{a}} = \mathcal{A}_{\bar{a}a} = \int_{k_{\min}^n}^{\infty} \int_{k_{\min}^o}^{\infty} dk_n dk_o P_d(k_n) P_d(k_o) \frac{(1 - \mathcal{T}_2^2 \mathcal{T}_4)(1 + \mathcal{T}_4)}{(1 + \mathcal{T}_2^2 \mathcal{T}_4)^2 \cosh^2(K_2(m_o k_o + m_n k_n))} k_n k_o, \quad (\text{B2})$$

$$\mathcal{A}_{aM} = \int_{k_{\min}^n}^{\infty} \int_{k_{\min}^o}^{\infty} dk_n dk_o P_d(k_n) P_d(k_o) \frac{(1 - \mathcal{T}_2^2) \mathcal{T}_4}{(1 + \mathcal{T}_2^2 \mathcal{T}_4)^2 \cosh^2(K_4 M k_o)} k_a k_o, \quad (\text{B3})$$

$$\mathcal{A}_{Ma} = \int_{k_{\min}^n}^{\infty} \int_{k_{\min}^o}^{\infty} dk_n dk_o P_d(k_n) P_d(k_o) \frac{2\mathcal{T}_2(1 - \mathcal{T}_4^2)}{(1 + \mathcal{T}_2^2 \mathcal{T}_4)^2 \cosh^2(K_2(m_o k_o + m_n k_n))} k_o k_a, \quad (\text{B4})$$

$$\mathcal{A}_{MM} = \int_{k_{\min}^n}^{\infty} \int_{k_{\min}^o}^{\infty} dk_n dk_o P_d(k_n) P_d(k_o) \frac{1 - \mathcal{T}_2^4}{(1 + \mathcal{T}_2^2 \mathcal{T}_4)^2 \cosh^2(K_4 M k_o)} k_o^2. \quad (\text{B5})$$

Appendix C: Definitions of coefficients in free energy density

The coefficients C and D are defined as follows:

$$\begin{aligned} C_o(\lambda_o) &= C_M(\lambda_o) = -N_o \int_0^{\infty} \left[\ln(\cosh y) - \frac{1}{2} y^2 \right] y^{-\lambda_o} dy, \\ C_n(\lambda_n) &= -N_n \int_0^{\infty} \left[\ln(\cosh y) - \frac{1}{2} y^2 \right] y^{-\lambda_n} dy, \\ D_m(\lambda_o) &= -N_o \int_0^{\infty} y \ln(1 + \tanh^2 y) y^{-\lambda_o} dy, \\ D_M(\lambda_o) &= -N_o \int_0^{\infty} y^2 \ln(1 + \tanh y) y^{-\lambda_o} dy, \\ D_0(r_o, \lambda_o) &= -N_o \int_0^{\infty} \ln(1 + \tanh^2 y \tanh(r_o y)) y^{-\lambda_o} dy, \\ C_o(r_o, \lambda_o) &= C_o(\lambda_o) + D_0(r_o, \lambda_o) + \frac{1}{2} C_M(\lambda_o). \end{aligned} \quad (\text{C1})$$

Appendix D: Free energy of the Ising model on multiplex networks

The free energy f are written more precisely as follows:

(i) For $x < x_M$ and $\lambda_n > \lambda_o$,

$$\begin{aligned} f(m_o) &\simeq -\frac{K_2 \langle k_n \rangle^2 K_2 \langle k_o \rangle^2}{\langle k_n \rangle - K_2 \langle k_n^2 \rangle} K_2 m_o^2 + (\langle k_o \rangle - K_2 \langle k_o^2 \rangle) K_2 m_o^2 + C_o(\lambda_o) (K_2 m_o)^{\lambda_o-1} + C_n(\lambda_n) \left(\frac{K_2 \langle k_n \rangle K_2 \langle k_o \rangle}{\langle k_n \rangle - K_2 \langle k_n^2 \rangle} m_o \right)^{\lambda_n-1} \\ &\quad - \frac{1}{2} \frac{K_4 [D_m(\lambda_o)]^2}{\langle k_o \rangle [1 - x T_s / (x_M T)]} (K_2 m_o)^{2(\lambda_o-2)} - \frac{K_2 [(\lambda_n - 1) C_n(\lambda_n)]^2}{\langle k_n \rangle - K_2 \langle k_n^2 \rangle} \left(\frac{K_2 \langle k_n \rangle K_2 \langle k_o \rangle}{\langle k_n \rangle - K_2 \langle k_n^2 \rangle} m_o \right)^{2(\lambda_n-2)} + \text{h.o.} \end{aligned} \quad (\text{D1})$$

(ii) For $x < x_M$ and $\lambda_n < \lambda_o$,

$$f(m_n) \simeq -\frac{K_2 \langle k_n \rangle^2 K_2 \langle k_o \rangle^2}{\langle k_o \rangle - K_2 \langle k_o^2 \rangle} K_2 m_n^2 + (\langle k_n \rangle - K_2 \langle k_n^2 \rangle) K_2 m_n^2 + C_n(\lambda_n)(K_2 m_n)^{\lambda_n-1} + C_o(\lambda_o) \left(\frac{K_2 \langle k_n \rangle K_2 \langle k_o \rangle}{\langle k_o \rangle - K_2 \langle k_o^2 \rangle} m_n \right)^{\lambda_o-1} \\ - \frac{1}{2} \frac{K_4 [D_m(\lambda_o)]^2}{\langle k_o \rangle [1 - x T_s / (x_M T)]} \left(\frac{K_2 \langle k_n \rangle K_2 \langle k_o \rangle}{\langle k_o \rangle - K_2 \langle k_o^2 \rangle} m_n \right)^{2(\lambda_o-2)} - \frac{K_2 [(\lambda_o - 1) C_o(\lambda_o)]^2}{\langle k_o \rangle - K_2 \langle k_o^2 \rangle} \left(\frac{K_2 \langle k_n \rangle K_2 \langle k_o \rangle}{\langle k_o \rangle - K_2 \langle k_o^2 \rangle} m_n \right)^{2(\lambda_o-2)} + \text{h.o.} \quad (\text{D2})$$

(iii) For $x > x_M$ and $\lambda_n > \lambda_o$,

$$f(m_o) \simeq f_o(M_*) - \frac{(1 + K_4 M_* \langle k_o^2 \rangle / \langle k_o \rangle)^2 K_2 \langle k_n \rangle^2 K_2 \langle k_o \rangle^2}{\langle k_n \rangle [1 - K_2 (\langle k_n^2 \rangle / \langle k_n \rangle + g_n(M_*))]} K_2 m_o^2 + \langle k_o \rangle \left[1 - K_2 \left(\frac{\langle k_o^2 \rangle}{\langle k_o \rangle} + g_o(M_*) \right) \right] K_2 m_o^2 \\ + C_o(\lambda_o)(K_2 m_o)^{\lambda_o-1} + C_n(\lambda_n) \left[\frac{(1 + K_4 M_* \langle k_o^2 \rangle / \langle k_o \rangle) K_2 \langle k_n \rangle K_2 \langle k_o \rangle}{\langle k_n \rangle [1 - K_2 (\langle k_n^2 \rangle / \langle k_n \rangle + g_n(M_*))]} m_o \right]^{\lambda_n-1} \\ - \frac{K_2 [(\lambda_n - 1) C_n(\lambda_n)]^2}{\langle k_n \rangle [1 - K_2 (\langle k_n^2 \rangle / \langle k_n \rangle + g_n(M_*))]} \left[\frac{(1 + K_4 M_* \langle k_o^2 \rangle / \langle k_o \rangle) K_2 \langle k_n \rangle K_2 \langle k_o \rangle}{\langle k_n \rangle [1 - K_2 (\langle k_n^2 \rangle / \langle k_n \rangle + g_n(M_*))]} m_o \right]^{2(\lambda_n-2)} \\ - \frac{1}{2} (\lambda_o - 3) \frac{K_4 [D_M(\lambda_o)(K_4 M_*)^{\lambda_o-4}]^2}{\langle k_o \rangle (T_{s,M} / T - 1)} (K_2 m_o)^4 + \text{h.o.} \quad (\text{D3})$$

(iv) For $x \geq x_M$ and $\lambda_n < \lambda_o$,

$$f(m_n) \simeq f_o(M_*) - \frac{(1 + K_4 M_* \langle k_o^2 \rangle / \langle k_o \rangle)^2 K_2 \langle k_n \rangle^2 K_2 \langle k_o \rangle^2}{\langle k_o \rangle [1 - K_2 (\langle k_o^2 \rangle / \langle k_o \rangle + g_o(M_*))]} K_2 m_n^2 + \langle k_n \rangle \left[1 - K_2 \left(\frac{\langle k_n^2 \rangle}{\langle k_n \rangle} + g_n(M_*) \right) \right] K_2 m_n^2 \\ + C_n(\lambda_n)(K_2 m_n)^{\lambda_n-1} + C_o(\lambda_o) \left[\frac{(1 + K_4 M_* \langle k_o^2 \rangle / \langle k_o \rangle) K_2 \langle k_n \rangle K_2 \langle k_o \rangle}{\langle k_o \rangle [1 - K_2 (\langle k_o^2 \rangle / \langle k_o \rangle + g_o(M_*))]} m_n \right]^{\lambda_o-1} \\ - \frac{K_2 [(\lambda_o - 1) C_o(\lambda_o)]^2}{\langle k_o \rangle [1 - K_2 (\langle k_o^2 \rangle / \langle k_o \rangle + g_o(M_*))]} \left[\frac{(1 + K_4 M_* \langle k_o^2 \rangle / \langle k_o \rangle) K_2 \langle k_n \rangle K_2 \langle k_o \rangle}{\langle k_o \rangle [1 - K_2 (\langle k_o^2 \rangle / \langle k_o \rangle + g_o(M_*))]} m_n \right]^{2(\lambda_o-2)} \\ - \frac{1}{2} (\lambda_o - 3) \frac{K_4 [D_M(\lambda_o)(K_4 M_*)^{\lambda_o-4}]^2}{\langle k_o \rangle (T_{s,M} / T - 1)} \left[\frac{(1 + K_4 M_* \langle k_o^2 \rangle / \langle k_o \rangle) K_2 \langle k_n \rangle K_2 \langle k_o \rangle}{\langle k_o \rangle [1 - K_2 (\langle k_o^2 \rangle / \langle k_o \rangle + g_o(M_*))]} m_n \right]^4 + \text{h.o.}, \quad (\text{D4})$$

where $g_n(M_*) \langle k_n \rangle = K_4 M_* \langle k_o \rangle \langle k_n^2 \rangle$, $g_o(M_*) \langle k_o \rangle = D_M(\lambda_o)(K_4 M_*)^{\lambda_o-3} - \int_0^1 \tanh(K_4 M_* k_o) k_o^2 P_d(k_o) \, dk_o$.

(v) For $x = x_M$ and $\lambda_n > \lambda_o$,

$$\begin{aligned}
f(m_o) \simeq & -\frac{K_2 \langle k_n \rangle^2 K_2 \langle k_o \rangle^2}{\langle k_n \rangle - K_2 \langle k_n^2 \rangle} K_2 m_o^2 + (\langle k_o \rangle - K_2 \langle k_o^2 \rangle) K_2 m_o^2 + \frac{1}{2} (\langle k_o \rangle - K_4 \langle k_o^2 \rangle) K_4 M^2 \\
& + C_o(\lambda_o)(K_2 m_o)^{\lambda_o-1} + D_0(r_0, \lambda_o)(K_2 m_o)^{\lambda_o-1} + \frac{1}{2} C_M(\lambda_o)(K_4 M)^{\lambda_o-1} + C_n(\lambda_n) \left(\frac{K_2 \langle k_n \rangle K_2 \langle k_o \rangle}{\langle k_n \rangle - K_2 \langle k_n^2 \rangle} m_o \right)^{\lambda_n-1} \\
& - 2(K_4 M) \left(\frac{K_2 \langle k_n \rangle K_2 \langle k_o \rangle}{\langle k_n \rangle - K_2 \langle k_n^2 \rangle} m_o \right) (K_2 m_o) \langle k_n \rangle \langle k_o^2 \rangle - (K_4 M) \left(\frac{K_2 \langle k_n \rangle K_2 \langle k_o \rangle}{\langle k_n \rangle - K_2 \langle k_n^2 \rangle} m_o \right)^2 \langle k_n^2 \rangle \langle k_o \rangle - \frac{\lambda_o - 1}{\lambda_o - 4} k_o^4 (K_4 M) (K_2 m_o)^2 \\
& - \frac{K_2 [(\lambda_n - 1) C_n(\lambda_n)]^2}{\langle k_n \rangle - K_2 \langle k_n^2 \rangle} \left(\frac{K_2 \langle k_n \rangle K_2 \langle k_o \rangle}{\langle k_n \rangle - K_2 \langle k_n^2 \rangle} m_o \right)^{2(\lambda_n-2)} + \text{h.o.} .
\end{aligned} \tag{D5}$$

Appendix E: Susceptibility near the critical temperature

1. m_a - magnetization

a. for $x < x_M$

Now, we consider the susceptibility at the critical temperature T_s for weak interlayer interaction $x < x_M$ case. We can omit the higher order terms in m_a and M when m_a and M are very small, we expand the self-consistency relations for m_a (A2) with respect to m_a and M as follows:

$$m_a \langle k_a \rangle \simeq \Omega_a \langle k_a^2 \rangle + \Omega_{\bar{a}} \langle k_o \rangle \langle k_n \rangle - (\lambda_a - 1) C_a(\lambda_a) (\Omega_a)^{\lambda_a-2} . \tag{E1}$$

To obtain critical exponent γ for each m_a -magnetization repectively, we consider the lowest-order terms of the self-consistency relations Eqs. (E1) and then we obtain the following:

$$\begin{aligned}
m_a \langle k_n \rangle \langle k_o \rangle \left(1 - \frac{T_\ell}{T} \right) \left(1 - \frac{T_s}{T} \right) \simeq & E_{\bar{a}} \left(H_a \langle k_a^2 \rangle + H_{\bar{a}} \langle k_o \rangle \langle k_n \rangle - (\lambda_a - 1) C_a(\lambda_a) (\Omega_a)^{\lambda_a-2} \right) \\
& + F_{a\bar{a}} \left(H_{\bar{a}} \langle k_a^2 \rangle + H_a \langle k_a \rangle \langle k_{\bar{a}} \rangle - (\lambda_{\bar{a}} - 1) C_{\bar{a}}(\lambda_{\bar{a}}) (\Omega_{\bar{a}})^{\lambda_{\bar{a}}-2} \right) + \text{h.o.} ,
\end{aligned} \tag{E2}$$

where $E_{\bar{a}} = \langle k_{\bar{a}} \rangle \left(1 - \frac{\langle k_{\bar{a}}^2 \rangle / \langle k_{\bar{a}} \rangle}{T} \right)$ and $F_{a\bar{a}} = \frac{1}{T} \langle k_o \rangle \langle k_n \rangle$.

In order to derive the susceptibility from magnetization, we take partial derivative with respect to H_a and then take the H_a and $H_{\bar{a}} \rightarrow 0$ limit. We have two equations for susceptibility as follows:

$$\begin{aligned}
\chi_a \langle k_a \rangle \langle k_{\bar{a}} \rangle \left(1 - \frac{T_\ell}{T} \right) \left(1 - \frac{T_s}{T} \right) \simeq & E_{\bar{a}} \left(\langle k_a^2 \rangle - (\lambda_a - 1)(\lambda_a - 2) C_a(\lambda_a) (K_2 m_a)^{\lambda_a-3} K_2 \chi_a \right) \\
& + F \left(\langle k_a \rangle \langle k_{\bar{a}} \rangle - (\lambda_{\bar{a}} - 1)(\lambda_{\bar{a}} - 2) C_{\bar{a}}(\lambda_{\bar{a}}) (K_2 m_{\bar{a}})^{\lambda_{\bar{a}}-3} K_2 \frac{\partial m_{\bar{a}}}{\partial H_{\bar{a}}} \right) + \text{h.o.} .
\end{aligned} \tag{E3}$$

When $\lambda_o < \lambda_n$, the susceptibility near the critical temperature T_s^- is written as follows:

$$\begin{aligned}
\chi_o \langle k_n \rangle \langle k_o \rangle \left(1 - \frac{T_\ell}{T} \right) \left(1 - \frac{T_s}{T} \right) \approx & E_n \langle k_o^2 \rangle + F \langle k_o \rangle \langle k_n \rangle + (\lambda_o - 2) \langle k_o \rangle \langle k_n \rangle \left(1 - \frac{T_\ell}{T} \right) \left(1 - \frac{T_s}{T} \right) \chi_o + \text{h.o.} , \\
\chi_n \langle k_n \rangle \langle k_o \rangle \left(1 - \frac{T_\ell}{T} \right) \left(1 - \frac{T_s}{T} \right) \approx & E_o \langle k_n^2 \rangle + F \langle k_o \rangle \langle k_n \rangle + (\lambda_o - 2) \langle k_o \rangle \langle k_n \rangle \left(1 - \frac{T_\ell}{T} \right) \left(1 - \frac{T_s}{T} \right) \frac{E_o}{E_n} \frac{\partial m_o}{\partial H_n} + \text{h.o.} .
\end{aligned} \tag{E4}$$

To obtain the susceptibility near T_s^- , we use the following relation

$$E_n \left(-(\lambda_o - 1) K_2 C_o(\lambda_o) (K_2 m_o)^{\lambda_o-3} \right) \approx \langle k_o \rangle \langle k_n \rangle \left(1 - \frac{T_\ell}{T} \right) \left(1 - \frac{T_s}{T} \right) \text{ for } T \rightarrow T_s^- . \tag{E5}$$

To get χ_n , we need to compute the $\partial m_o / \partial H_n$ term. The partial derivative of m_o in terms of H_n is given as follows:

$$\begin{aligned} \frac{\partial m_o}{\partial H_n} \langle k_o \rangle \langle k_n \rangle (1 - \frac{T_\ell}{T})(1 - \frac{T_s}{T}) &\simeq E_n \left(\langle k_o \rangle \langle k_n \rangle + (\lambda_o - 1)(\lambda_o - 2)C_o(\lambda_o)(K_2 m_o)^{\lambda_o - 3} K_2 \frac{\partial m_o}{\partial H_n} \right) + F \langle k_n^2 \rangle + \text{h.o.} \\ &\simeq E_n \langle k_o \rangle \langle k_n \rangle + F \langle k_n^2 \rangle + (\lambda_o - 2) \langle k_o \rangle \langle k_n \rangle (1 - \frac{T_\ell}{T})(1 - \frac{T_s}{T}) \frac{\partial m_o}{\partial H_n} + \text{h.o.} \dots \end{aligned} \quad (\text{E6})$$

From Eq. (E6), we obtain that $\partial m_o / \partial H_n \approx (T_s - T)^{-1}$ for $T \rightarrow T_s^-$. Using this, the susceptibility of m_a is obtained as

$$\chi_o \approx \begin{cases} (T - T_s)^{-1} & \text{for } T_s^+, \\ (T_s - T)^{-1} & \text{for } T_s^-, \end{cases} \quad \text{and} \quad \chi_n \approx \begin{cases} (T - T_s)^{-1} & \text{for } T_s^+, \\ (T_s - T)^{-1} & \text{for } T_s^-. \end{cases} \quad (\text{E7})$$

Here, we take the limit $m_o \rightarrow 0$ for near T_s^+ to Eq.(E3). For the $\lambda_n < \lambda_o$ case, the susceptibility of m_a is obtained by similar computation process same as for the $\lambda_o < \lambda_n$ case. Thus, the critical exponent of $\gamma_{m\pm}$ of magnetization are always 1 for all cases. Then, the scaling relation, $a + 2\beta_m + \gamma_{m-} = 2$, is satisfied for each m_a -magnetization, respectively.

Now, we compute the susceptibility at CE point as boundary point of continuous PT regime. Since the location of magnetization jumps to a certain finite at the CE, the magnitude of the magnetization is much greater than 0, the perturbative expansions with respect to m, M is not valid any longer at CE point. Thus, we should keep the integral formula written in self-consistent relation Eqs. (A2) and (A3) as follows. In order to obtain the susceptibility for m_a magnetization, we take a partial derivative of self-consistent relation for m_a (A2) with respect of H_2 and take $H_2, H_4 \rightarrow 0$ limit, then the susceptibility is written as follows:

$$\chi_o = \frac{\mathcal{A}_{oo} + \mathcal{A}_{on} K_2 \partial m_n / \partial H_o + \mathcal{A}_{oM} K_4 \partial M / \partial H_o}{\langle k_o \rangle - K_2 \mathcal{A}_{oo}}, \quad (\text{E8})$$

To evaluate Eq. (E8), we also should compute the

$$\left. \frac{\partial m_n}{\partial H_o} \right|_{H_a, H_4 \rightarrow 0} \quad \text{and} \quad \left. \frac{\partial M}{\partial H_o} \right|_{H_a, H_4 \rightarrow 0} \quad (\text{E9})$$

terms. Thus, we firstly take a derivative of self-consistent relation for m_n and M (A2),(A3) with respect to H_o and then take the limit H_a and $H_4 \rightarrow 0$, we obtain as follows:

$$\frac{\partial m_n}{\partial H_o} = \frac{\mathcal{A}_{no} + \mathcal{A}_{no} K_2 \chi_o + \mathcal{A}_{nM} K_4 \partial M / \partial H_o}{\langle k_n \rangle - K_2 \mathcal{A}_{nn}}, \quad \frac{\partial M}{\partial H_o} = \frac{\mathcal{A}_{Mo} + \mathcal{A}_{Mo} K_2 \chi_o + \mathcal{A}_{Mn} K_2 \partial m_n / \partial H_o}{\langle k_o \rangle - K_4 \mathcal{A}_{MM}} \quad (\text{E10})$$

At CE, χ_o is computed similarly to Eq. (E3) at T_s^+ , where $m_a = M = 0$. For T_s^- , χ_m can be obtained numerically from Eqs. (E8), (E10). We can confirm that the susceptibility has a certain finite value at T_s^- by numerical computations.

b. for $x > x_M$

Otherwise, for $x > x_M$ case, we expand the self-consistency relations for m_a with respect to m_a and M as follows:

$$\begin{aligned} m_a \langle k_n \rangle \langle k_o \rangle (1 - \frac{T'_\ell}{T})(1 - \frac{T'_s}{T}) &\simeq E'_a \left[H_a \langle k_a^2 \rangle + H_{\bar{a}} \langle k_o \rangle \langle k_n \rangle - (\lambda_a - 1)C_a(\lambda_a)(\Omega_a)^{\lambda_a - 2} \right] \\ &+ F'_{a\bar{a}} \left[H_{\bar{a}} \langle k_a^2 \rangle + H_a \langle k_a \rangle \langle k_{\bar{a}} \rangle - (\lambda_{\bar{a}} - 1)C_{\bar{a}}(\lambda_{\bar{a}})(\Omega_{\bar{a}})^{\lambda_{\bar{a}} - 2} \right] + \text{h.o.}, \end{aligned} \quad (\text{E11})$$

where $E'_a = \langle k_{\bar{a}} \rangle \left(1 - \frac{\langle k_a^2 \rangle / \langle k_{\bar{a}} \rangle + g_{\bar{a}}(M_*)}{T} \right)$ and $F'_{a\bar{a}} = \frac{1}{T} \langle k_o \rangle \langle k_n \rangle + \frac{1}{T} K_4 M_* \langle k_o^2 \rangle \langle k_n \rangle$.

It can be checked easily that Eq. (E11) is similar case to Eq. (E2) except the critical temperature T'_s and coefficients E'_a and F' . Thus, we performed similar calculations as for $x < x_M$ case considering minor differences between $x < x_M$ and $x > x_M$ cases. By performing similar calculations as for $x < x_M$ case, we obtain the susceptibility of m_a as follows:

$$\chi_o \approx \begin{cases} (T - T'_s)^{-1} & \text{for } T > T'_s, \\ (T'_s - T)^{-1} & \text{for } T'_s > T. \end{cases} \quad \text{and} \quad \chi_n \approx \begin{cases} (T - T'_s)^{-1} & \text{for } T > T'_s, \\ (T'_s - T)^{-1} & \text{for } T'_s > T. \end{cases} \quad (\text{E12})$$

2. M - magnetization

Likewise, the self-consistency relation for M (A3) can be expanded as

$$M\langle k_o \rangle \simeq \Omega_4 \langle k_o^2 \rangle - (\lambda_o - 1)C_M(\lambda_o)\Omega_4^{\lambda_o-2} - D_m(\lambda_o)\Omega_{\lambda_o-2} + \text{h.o.} \quad (\text{E13})$$

To obtain the susceptibility of M , we take partial derivative of the above self-consistency relation with respect to H_4 and then taking H_2 and $H_4 \rightarrow 0$.

$$\chi_M \langle k_o \rangle \simeq (K_4 \chi_M + 1) \langle k_o^2 \rangle - (\lambda_o - 2)C_M(\lambda_o)(K_4 \chi_M)(K_4 M)^{\lambda_o-3} - (\lambda_o - 2)D_m(\lambda_o)(K_2 m_o)^{\lambda_o-3} K_2 \frac{\partial m_o}{\partial H_4} + \text{h.o.} \quad (\text{E14})$$

For $x < x_M$, M is given as order of $m_o^{\lambda_o-2}$ and so $\partial m_o / \partial H_4$ is very small compared with the $O(1)$ term. Taking this limit, we obtain the susceptibility of M . We also take the limit $m_o = 0$ for $T_{s,M}^+$.

$$\chi_M \approx \left(T - x \frac{\langle k_o^2 \rangle}{\langle k_o \rangle} \right)^{-1} \quad (\text{E15})$$

Otherwise, $x \geq x_M$ and $T \rightarrow T_{s,M}^-$, M can be approximated to M_* , where M_* becomes Ising spin in single SF networks, and m_a is negligible to M . Taking this limit, we can obtain the susceptibility of M as follow. We also take the limit $M = 0$ for $T_{s,M}^+$.

$$\chi_M \approx \begin{cases} (T - T_{s,M})^{-1} & \text{for } T > T_{s,M}, \\ (T_{s,M} - T)^{-1} & \text{for } T_{s,M} > T. \end{cases} \quad (\text{E16})$$

ACKNOWLEDGMENTS

This research was supported by the NRF, Grant No. NRF-2014R1A3A2069005 (BK).

-
- [1] A.-L. Barabási, *Network Science* (Cambridge, Cambridge University Press, 2016).
 - [2] S. N. Dorogovtsev, *Lectures on complex networks* (Oxford, Oxford University Press, 2010).
 - [3] M. Newman, *Networks: an introduction* (Oxford, Oxford University Press, 2010).
 - [4] D. Lee, B. Kahng, Y.S. Cho, K.-I. Goh, and D.-S. Lee, *J. Korean Phys. Soc.* **73**, 152-164 (2018).
 - [5] S. N. Dorogovtsev, A. V. Goltsev, and J. F. F. Mendes, *Rev. Mod. Phys.* **80**, 1275 (2008).
 - [6] G. Bianconi, *Multilayer networks: structure and function* (Oxford University Press, 2018).
 - [7] S. V. Buldyrev, R. Parshani, G. Paul, H. E. Stanley, and S. Havlin, *Nature (London)* **464**, 1025 (2010).
 - [8] S. Boccaletti, G. Bianconi, R. Criado, C. I. del Genio, J. Gómez-Gardeñes, M. Romance, I. Sendiña-Nadal, Z. Wang, and M. Zanin, *Phys. Rep.* **544**, 1 (2014).
 - [9] M. Kivelä, A. Arenas, M. Barthelemy, J. P. Gleeson, Y. Moreno, and M. A. Porter, *J. Complex Netw.* **2**, 203 (2014).
 - [10] K.-M. Lee, B. Min, and K.-I. Goh, *Eur. Phys. Jour. B* **88**, 1 (2015).
 - [11] M. Szell, R. Lambiotte, and S. Thurner, *Proc. Natl. Acad. Sci. U.S.A.* **107**, 13636 (2010).
 - [12] G. Menichetti, D. Remondini, P. Panzarasa, R. J. Mondragón, and G. Bianconi, *PloS one* **9**, e97857 (2014).
 - [13] A. Cardillo, J. Gómez-Gardeñes, M. Zanin, M. Romance, D. Papo, F. del Pozo, and S. Boccaletti, *Sci. Rep.* **3**, 1344 (2013).
 - [14] E. Bullmore and O. Sporns, *Nat. Rev. Neurosci.* **10**, 186 (2009).
 - [15] S. D. S. Reis, Y. Hu, A. Babino, J. S. Andrade Jr., S. Canals, M. Sigman, and H. A. Makse, *Nat. Phys.* **10**, 762 (2014).
 - [16] G. Bianconi, *Phys. Rev. E* **87**, 062806 (2013).
 - [17] B. Min, S. D. Yi, K.-M. Lee, and K.-I. Goh, *Phys. Rev. E* **89**, 042811 (2014).
 - [18] V. Nicosia, V. Latora, *Phys. Rev. E* **92**, 032805 (2015).
 - [19] H. Wu, R. G. James, R. M. D'Souza *Jour. Comp. Net.* **8**, 2 (2020).
 - [20] S. V. Buldyrev, R. Parshani, G. Paul, H. E. Stanley, and S. Havlin, *Nature* **464**, 1025 (2010).
 - [21] G. J. Baxter, S. N. Dorogovtsev, A. V. Goltsev, and J. F. F. Mendes, *Phys. Rev. Lett.* **109**, 248701 (2012).
 - [22] S. Hwang, S. Choi, D. Lee, and B. Kahng, *Phys. Rev. E* **91**, 022814 (2015).
 - [23] G. Bianconi, S. N. Dorogovtsev, and J. F. F. Mendes, *Physical Review E* **91**, 012804 (2015).
 - [24] S. Gómez, A. Díaz-Guilera, J. Gómez-Gardeñes, C. J. Pérez-Vicente, Y. Moreno, and A. Arenas, *Phys. Rev. Lett.* **110**, 028701 (2013).
 - [25] M. De Domenico, A. Solé-Ribalta, S. Gómez, and A. Arenas, *Proc. Natl. Acad. Sci. U.S.A.* **111**, 8351 (2014).
 - [26] A. Saumell-Mendiola, M. A. Serrano, and M. Boguna, *Phys.*

- Rev. E **86**, 026106 (2012).
- [27] E. Cozzo, R. A. Banos, S. Meloni, and Y. Moreno, Phys. Rev. E **88**, 050801(R) (2013).
 - [28] C. Granell, S. Gómez, and A. Arenas, Phys. Rev. Lett. **111**, 128701 (2013).
 - [29] Z. Wang, L. Wang, A. Szolnoki, and M. Perc, Eur. Phys. Jour. B **88**, 1 (2015).
 - [30] M. Perc, J. Gómez-Gardeñes, A. Szolnoki, L. M. Floría, and Y. Moreno, J. R. Soc. Interface **10**, 20120997 (2013).
 - [31] N. Masuda, Phys. Rev. E **90**, 012802 (2014).
 - [32] M. Diakonova, M. San Miguel, and V. M. Eguíluz, Phys. Rev. E **89**, 062818 (2014).
 - [33] M. Diakonova, V. Nicosia, V. Latora, and M. San Miguel, New J. Phys. **18**, 023010 (2016).
 - [34] A. Halu, K. Zhao, A. Baronchelli, and G. Bianconi, Europhys. Lett. **102**, 16002 (2013).
 - [35] F. Battiston, A. Cairoli, V. Nicosia, A. Baule, and V. Latora, Physica D 323-324, 12 (2016).
 - [36] J. Ashkin and E. Teller, Phys. Rev. **64**, 178 (1943).
 - [37] S. Jang, J.S. Lee, S. Hwang, B. Kahng, Phys. Rev. E **92**, 022110 (2015).
 - [38] R.V. Ditzian and L. P. Kadanoff, J. Phys. A **12**, L229 (1979).
 - [39] Sang Hoon Lee, Meesoon Ha, Hawoong Jeong, Jae Dong Noh and Hyunggyu Park, Phys. Rev. E **80**, 051127 (2009).
 - [40] Ferenc Igloi and Loïc Turban, Phys. Rev. E **66**, 036140 (2002).
 - [41] S. N. Dorogovtsev, A. V. Goltsev, and J. F. F. Mendes, Eur. Phys. J. B **38**, 177-182 (2004).